

Mangrove-Habitat Expansion in the Southern Firth of Thames: Sedimentation Processes and Coastal-Hazards Mitigation

Prepared by:
by National Institute of Water & Atmospheric Research Ltd

For:
Environment Waikato
PO Box 4010
HAMILTON EAST

June 2007

Peer reviewed by:
Vernon Pickett

Date February 2008

Approved for release by:
Peter Singleton

Date February 2008

Disclaimer

This technical report has been prepared for the use of Waikato Regional Council as a reference document and as such does not constitute Council's policy.

Council requests that if excerpts or inferences are drawn from this document for further use by individuals or organisations, due care should be taken to ensure that the appropriate context has been preserved, and is accurately reflected and referenced in any subsequent spoken or written communication.

While Waikato Regional Council has exercised all reasonable skill and care in controlling the contents of this report, Council accepts no liability in contract, tort or otherwise, for any loss, damage, injury or expense (whether direct, indirect or consequential) arising out of the provision of this information or its use by you or any other party.

**Mangrove-habitat expansion in the southern Firth of Thames:
sedimentation processes and coastal-hazards mitigation.**



**NIWA Client Report: HAM2006-138
June 2007**

NIWA Project: EVW06208

Mangrove-habitat expansion in the southern Firth of Thames: sedimentation processes and coastal-hazards mitigation.

A. Swales
R.G. Bell
R. Ovenden
C. Hart
M. Horrocks¹
N. Hermanspahn²
R. K. Smith³

(1) Microfossil Research Ltd
(2) National Radiation Laboratory
(3) Coastal Consultant

Prepared for

Environment Waikato

NIWA Client Report: HAM2006-138
June 2007

NIWA Project: EVW06208

National Institute of Water & Atmospheric Research Ltd
Gate 10, Silverdale Road, Hamilton
P O Box 11115, Hamilton, New Zealand
Phone +64-7-856 7026, Fax +64-7-856 0151
www.niwa.co.nz

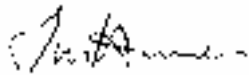
© All rights reserved. This publication may not be reproduced or copied in any form without the permission of the client. Such permission is to be given only in accordance with the terms of the client's contract with NIWA. This copyright extends to all forms of copying and any storage of material in any kind of information retrieval system.

Contents

Executive Summary	iv
1. Introduction	1
1.1 Firth of Thames - mangrove-habitat expansion	1
1.2 Role of mangroves in coastal-hazards mitigation	3
1.3 Study objectives	4
1.4 Report outline	4
2. Study area and hazards	5
2.1 Physical setting	5
2.2 History	5
2.3 Hydrodynamic setting	6
2.3.1 Depths and mean level of the sea	6
2.3.2 Tides, currents and waves	6
2.4 Sedimentary setting	7
2.5 Tectonic setting and tsunami hazard	8
2.6 Storm-tide hazards	10
3. Methodology	14
3.1 Mangrove-habitat expansion	14
3.2 Shore-normal elevation profiles	14
3.3 Sedimentation	15
3.3.1 Sediment dating	17
3.3.2 X-radiographs	18
3.3.3 Sediment bulk density	19
3.3.4 Particle-size analysis	19
3.4 Tides and storm surge	20
4. Results	22
4.1 Mangrove-habitat expansion in the southern Firth	22
4.2 Tides, storm surge and large-scale geomorphology	28
4.3 Sedimentation	31
4.3.1 How might mangrove-habitat expansion affect sedimentation?	31
4.3.2 Sediment-core physical parameters	32
4.3.3 Site LC-3 (old-growth forest)	33
4.3.4 Site LC-4 (old-growth forest)	36
4.3.5 Site LC-5 (old-growth forest)	37
4.3.6 Site LC-6 (old-growth forest)	40
4.3.7 Site LC-7 (recent mangrove forest)	42
4.3.8 Site LC-8 (recent mangrove forest)	44
4.3.9 Site LC-9 (recent mangrove forest)	45
4.3.10 Site LC-10 (recent mangrove forest)	47
4.3.11 Site LC-11 (2005 forest fringe)	49
4.3.12 Site LC-12 (mudflat)	51
4.3.13 Pollen profiles	53
5. Synthesis	54
5.1 Overview	54
5.2 Mangrove-habitat expansion	55
5.3 Sedimentation processes	58
5.3.1 Particle-size changes	58
5.3.2 Sedimentation rates	59
5.3.3 ²¹⁰ Pb Budget and implications for fine-sediment fate	61
5.3.4 Pollen Chronology	63
5.4 Role of storms in mangrove-forest development	65

5.5	Mangrove colonisation: triggers, controls and future habitat expansion	70
5.6	Large-scale morphological evolution	72
5.7	Coastal-hazards mitigation by mangroves	77
5.7.1	Coastal erosion	77
5.7.2	Coastal Inundation	78
5.8	Future fate of the mangrove forest	85
6.	Summary	87
7.	Acknowledgements	93
8.	References	94
9.	Appendix One: Dating of estuarine sediments	103
9.1	Overview	103
9.2	¹³⁷ Cs dating	103
9.3	²¹⁰ Pb dating	104
9.3.1	Pollen dating	106
9.4	Sediment accumulation rates (SAR)	109
9.5	SAR from ²¹⁰ Pb dating	110
9.6	Sediment Mixing	111
10.	Appendix Two: Pollen Profiles	112

Reviewed by:



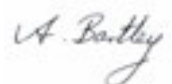
Terry Hume

Approved for release by:



David Roper

Formatting checked



Executive Summary

Introduction

Grey mangrove (*Avicennia marina* subsp. *australasica*) or Manawa has rapidly colonised intertidal areas of the southern Firth of Thames during the last 50 years or so. Today, mangrove habitat occupies some 7 km² of former intertidal flat between the Piako and Waitakaruru Rivers and 11 km² in the southern Firth as a whole (section 1). Grey-mangrove seedlings can colonise intertidal areas down to about mean sea level (MSL), where they are submerged for < six hours per tide. Mangrove-habitat expansion has occurred in many North Island estuaries in recent decades as sediments delivered by rivers has built intertidal habitat suitable for mangrove colonisation.

The Firth of Thames is an 800 km² meso-tidal estuarine embayment. Currents, sea level and waves within the Firth are strongly linked to oceanographic and meteorological processes occurring within the wider Hauraki Gulf (section 2). The low-lying coast of the southern Firth is potentially exposed to erosion and inundation due to sea and swell waves, storm surge and tsunami.

Environment Waikato commissioned NIWA to undertake a study of mangrove-habitat expansion and sedimentation processes in the southern Firth. The main objectives of the study are to:

- Reconstruct the historical sequence mangrove-habitat expansion based on historical aerial photography (1944–2005) and dated sediment cores.
- Quantify sediment accumulation rates (SAR) and changes in SAR resulting from mangrove colonisation and habitat expansion.
- Determine the role of mangrove habitat in mitigating coastal erosion and inundation hazards in the southern Firth.

Historical sequence of mangrove-habitat expansion

Aerial photographs show that mangrove stands were restricted to delta deposits at river mouths in the mid-1940s. We distinguish between **old-growth mangrove forest** that colonised the mudflats before the mid-1970s and **recent mangrove forest** that has established since that time (section 4.1). The boundary between these forests coincides with the seaward fringe of the forest in 1977 (i.e., site LC-6). The mangrove forest that has developed over the last 50 years is the result of only 4–5 major seedling-recruitment events that occurred in the early-1950s, mid-1960s, mid-1980s and early-1990s (Fig. 5.1). No major seedling recruitment has occurred in the last decade. Seedling mortality is primarily controlled by episodic wave-driven erosion of the mudflat and recruitment events are likely to coincide with extended periods of calm weather. This indicates a direct link between climate and mangrove-habitat expansion in the southern Firth of Thames.

The mangrove forest today at *c.* +1.7 m MSL is near the upper limit of the tide and is inundated < 3% of the time. The mean high water perigean spring (MHWPS) and MHWS tide levels are at +1.87 m MSL and +1.6 m MSL respectively. Storm tides increase the length of tidal inundation of the mangrove forest by *c.* 40% (i.e., 30 hrs/yr).

Sediment accumulation rates

The recent geomorphic evolution of the southern Firth is closely linked to historical increases in sediment loads following catchment deforestation and river-engineering works (1850s–1920s). An estimated 44 million m³ of mud was deposited in the southern Firth and lower Waihou River during a *c.* 40-year period up to 1918. Distributed evenly over the 200 km² of seabed the deposit would be *c.* 0.18 m thick. Below the base of the ≤ 1.6-m thick mud layer at *c.* +0.2-m MSL are the original laminated silts and sands that are characteristic of energetic mixed-sediment intertidal-flats. The transition to a mud substrate, which began in the 1920s, has initiated a sequence of large-scale environmental changes, which include the rapid mangrove-habitat expansion that began in the 1950s. Similar environmental changes have occurred in other New Zealand estuaries. However, the rate and magnitude of these changes has been much larger in the Firth.

The ²¹⁰Pb_{us} profiles show that sedimentation increased as mangroves colonised the mudflat then subsequently declined as the old-growth forest was progressively isolated from the mudflat by elevation and distance. Sediment accumulation rates (SAR) on the mudflat averaged *c.* 20 mm yr⁻¹ before mangroves arrived in the mid-1950s and is similar to rates on the mudflat today. For a time the mudflat seaward of the old-growth forest accumulated sediment 2–10 times more rapidly (30–90 mm yr⁻¹) and as much as 20 years before mangroves arrived in the mid-1980s. The seaward advance of the mangrove forest is preserved in the cores by the abrupt increase in SAR (50–200 mm yr⁻¹) that occurred on the forest fringe. ²¹⁰Pb inventories and particle-size data indicate that the mangrove-forest has preferentially accumulated fine sediment (section 5.3). We are unable to determine SAR based on the pollen profiles.

The recent geomorphic evolution of the mudflat and the mangrove forest in the southern Firth is reconstructed from the dated sediment cores, surface elevation profiles and aerial photographs (section 5.6). These data are summarised as age-surface elevation (ASE) curves for the old-growth and recent mangrove forests (Fig. 5.10). The elevation trajectories of the two forests have diverged markedly since the early 1980s. In the old-growth forest, average rates of surface-elevation change have declined and coincide with a progressive reduction in the duration of tidal inundation. In the recent forest, surface elevations have continued to increase rapidly until the present, which is consistent with the infilling of a large shallow basin in the forest over the last decade.

The aerial-photographs and sediment cores also preserve evidence of mudflat erosion and mangrove-forest damage by storms during the late 1970s (section 5.4). Loss of an estimated 35 hectares of mangrove forest occurred along the seaward fringe and extensive damage to *c.* 1.5 km² of forest. An

unconformity in the LC-6 $^{210}\text{Pb}_{\text{us}}$ concentration profile at 79–89-cm depth represents a storm event during which *c.* 0.4 m of vertical erosion occurred. This was sufficient to expose and detached the roots of mature mangrove trees from the mudflat. The most likely candidate storm is that which occurred in July 1978, which generated a 0.6-m storm surge and waves in the Firth that coincided with perigeon-spring high tides. A similar-magnitude storm in May 1938, which occurred before the mangrove forest existed, breached the stopbank in several places and the sea flooded *c.* 350 km² of the lower Hauraki Plains.

Presently, the seaward edge of the mangrove forest at *c.* +0.9 m MSL is 0.35 m above the lower-elevation limit for seedling recruitment on the wave-exposed mudflat (section 5.5). The mudflat slopes at 0.15° so that *c.* 150 metres of mudflat seaward of the mangrove-forest fringe is potentially immediately available for future mangrove-habitat expansion. Mudflat surface elevation is increasing at 25 mm yr⁻¹ so that the area suitable for mangrove seedlings increases by *c.* 10 m yr⁻¹. This estimate is similar to the average rate of mangrove-habitat expansion of 12.5 m yr⁻¹ over the last 50 years.

Coastal hazards mitigation

The mangrove forest provides a number of ecosystem services, which mitigate the potential coastal erosion and inundation hazards that exist for the low-lying Hauraki Plains. Farmland immediately behind the stopbank is *c.* 0.1 m below MSL and *c.* 2 m below the seabed elevation in the mangrove forest. Sediment accumulated in the mangrove forest provides an erosion buffer of *c.* 600 m³ per metre of shoreline. The potential for coastal erosion during large-magnitude storms is demonstrated by historical events (sections 2.6 and 5.4). The present-day mangrove-forest provides a high level of protection to the stopbank from wave-induced coastal erosion (section 5.7.1).

The risk of inundation relates to overtopping of the stopbank by extreme elevated sea levels and future sea-level rise (SLR) due to global warming (section 5.7.2). In making this inundation-hazard assessment, we assume a minimum stopbank crest level of *c.* +3.4 m MSL (Transect C) and that the mangrove forest is preserved. Inundation due to overtopping of the stopbank by storm tides or tsunami has the highest potential for large-scale and widespread damage to infrastructure and private property and direct impacts on the local economy. Although the mangrove forest will have a minimal effect on retarding the level of the high tide at the stopbank, extreme high tides will not cause inundation. Storm surge coinciding with high spring or perigeon (i.e., king) tides is also unlikely to cause overtopping at the surveyed transect locations. The likelihood of inundation by tsunami will depend on the height and period of the tsunami waves and the timing of the event with the astronomical tide. The forest would likely have a minimal effect on attenuating locally-generated short-period (e.g., 5 to 15 minute) tsunamis due to their shallow root systems but still provides a buffer to the dynamic component of tsunamis.

Since the mid 1800s, mean level of the sea around New Zealand has been rising (section 5.7.2). The long-term rate of relative sea level rise at Auckland (1899–2000) of 1.3 mm yr⁻¹ has increased to 1.4 mm yr⁻¹ (2001–2005). IPCC (2007) projections for sea-level rise (SLR) over the next 100 years range

from 1.8 to 8 mm yr⁻¹. In the southern Firth, SAR have averaged *c.* 20 mm yr⁻¹ on the bare mudflats over the last 50 years. The mangrove forest has accelerated sedimentation, with SAR averaging 50–100 mm yr⁻¹ on the forest fringe. SAR in the old-growth forest have reduced to 7–12 mm yr⁻¹ due to the infrequency of tidal inundation. Thus, sedimentation rates over the last 50 years have exceeded SLR predicted for the next 100 years by as much as a factor of ten. By comparison, SAR measured in Auckland, Waikato and Coromandel estuaries have averaged 2–4 mm yr⁻¹ over the last 50 years.

The fate of mangrove-forests primarily depends on sediment-surface elevation increasing at a rate equal to or exceeding SLR. This has previously been assessed by comparing sedimentation and SLR rates. However, this approach does not take into account the potential effects of sediment compaction and biotic factors, which also influence surface elevation. Mangrove systems are sensitive to changes in sea level because they depend on the maintenance of suitable upper-intertidal habitat. Mangroves can respond to rising sea levels by either maintaining sediment-surface elevation and/or retreating from the sea. In many estuaries, shore-protection structures preclude the retreat of mangrove forest from the rising sea. In the southern Firth, the mangrove forest can only respond to rising sea levels by maintaining surface elevation through sedimentation. This sedimentation process has implications for the efficacy of the stopbanks and maintenance of drainage.

There is some uncertainty in how the mangrove forests will respond to climate change and rising sea levels in the future due to the complex feedbacks between the physical and biological processes controlling substrate elevation. Future climate warming is likely to influence mangrove growth and productivity, rainfall patterns, catchment runoff, sediment loads, wave activity and storm-tide frequency. Sediment Elevation Tables (SET) have been widely used to monitor surface-elevation changes in mangrove forests and salt-marshes due to shallow subsidence and sedimentation (<http://www.pwrc.usgs.gov/set/>). SET have been installed in the mangrove forest by NIWA and Environment Waikato to provide basic information for research and management of mangrove forests.

1. Introduction

1.1 Firth of Thames - mangrove-habitat expansion

The mangrove (*Avicennia marina* subsp *australasica*) or Manawa has rapidly colonised intertidal areas of the southern Firth of Thames during the last 50 years or so (Fig. 1.1). Captain James Cook visited the Firth in 1769 and noted the presence of mangrove along the banks of the lower Waihou river (Beaglehole, 1968). Mangroves were present in the Firth at least 12,000 years ago. Sediment cores collected on the 35-m isobath west of Manaia (Coromandel Peninsula) contain mangrove pollen. These sediments were deposited on an earlier shoreline that existed 12,000 to 14,000 years ago as sea levels rose at the end of the Otira Glaciation (Pocknall et al. 1989).

Aerial photographs of the southern Firth in the 1940s and early 1950s show that mangrove-habitat was restricted to delta deposits flanking the mouths of the Waitakaruru, Piako and Waihou Rivers. Today, mangrove habitat occupies some 7 km² of former intertidal flat between the Piako and Waitakaruru Rivers and 11 km² in the southern Firth as a whole (Brownell, 2004).

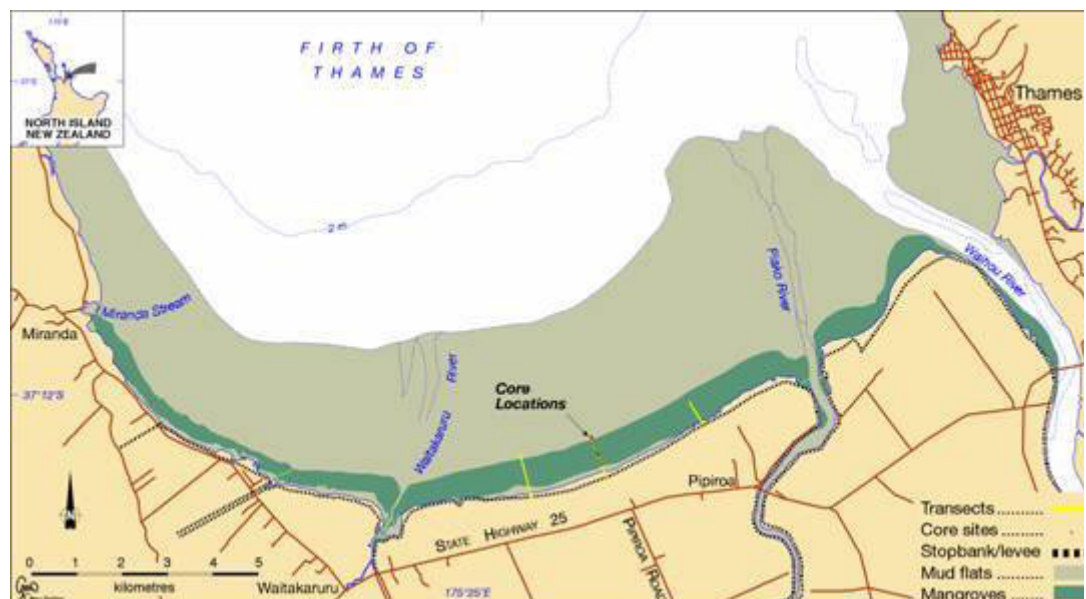


Figure 1.1: Location of the study area, southern Firth of Thames, New Zealand. Shore-normal elevation profiles at Transects A (east), B (opposite Pipiroa road) and C (west). Sediment cores collected along Transect B.

Manawa is a frost-sensitive species that occurs in North Island estuaries and on coastlines north of 38°S latitude. Their southern natural limits occur at Kutarere, Ohiwa Harbour, on the east coast and at Kawhia Harbour on the west coast.

Explanations for the geographic limits of mangroves in New Zealand include occurrence of ground frosts, current-driven propagule dispersal patterns and lack of suitable habitats (Crisp et al. 1990; de Lange and de Lange, 1994; Duke et al. 1998). Recent work by Beard (2006) suggests that mangrove distributions are also constrained by its physiological limitations at low (i.e., non-freezing) temperatures.

The distribution of grey mangroves within estuaries largely reflects the physiological limitations of their seedlings to tidal submersion. Seedlings can colonise intertidal areas down to about mean sea level (MSL) elevation, where they are submerged for no more than six hours per tidal cycle (Clarke and Myerscough, 1993). The lower-elevation limit for mangrove colonisation is also influenced by wave exposure. At wave-exposed sites in Tauranga Harbour, mangroves do not occur below *c.* +0.3 m MSL (Park, 2004). In the southern Firth, mangrove-seedling recruitment is strongly influenced by mud-flat erosion by waves and the infrequent recruitment events are likely to coincide with extended periods of calm weather (Swales et al. 2007). Thus, mangrove colonisation of estuaries influences, and is influenced by, the geomorphic processes of sedimentation and tidal-flat formation (Thom et al. 1975).

Mudflats and mangrove forests are most extensive in macrotidal embayments with limited wave exposure (Woodroffe, 2002). However, muddy coasts also develop under moderate wave-exposure where there is a large supply of fine sediment. Mangrove-habitat expansion has occurred in many North Island estuaries in recent decades (Burns and Ogden 1985; de Lange and de Lange 1994; Ellis et al. 2004). This process has been exacerbated by estuary sedimentation, which has accelerated over the last 150 years as catchment sediment loads have increased due to deforestation. Typically, sediment accumulation rates (SAR) of $< 0.5 \text{ mm yr}^{-1}$ before deforestation have increased by an order of magnitude or more (e.g., Hume and McGlone, 1986; Hume and Dahm, 1992; Goff, 1997; Swales et al. 1997; Swales et al. 2002; Odgen et al. 2007). These eroded sediments have built intertidal areas suitable for mangrove colonisation. Built structures such as causeways, road and rail embankments that alter hydrodynamic conditions may enhance sedimentation, thus providing suitable habitat for mangroves (Walsby, 1992).

An interesting feature of the estuary-infilling process is that mangrove-habitat expansion has largely occurred in the last several decades (e.g., Morrisey et al. 1999; Park, 2004; Young and Harvey, 1996). Alternative explanations suggested for this recent mangrove-habitat expansion include increased nutrient fluxes to estuaries associated with agricultural activities in catchments (Schwarz, 2002) and climatic factors that affect mangrove growth and propagule dispersal (de Lange and de Lange, 1994; McLeod and Salm, 2006).

Most North Island estuaries are enclosed, have high-tide surface areas of < 100 km² that are small relative to their land catchment. Consequently, physical conditions within these estuaries, such as water salinity and suspended sediment concentrations (SSC), are strongly influenced by catchment runoff. In contrast, the Firth is a large 800 km² estuarine embayment of the Hauraki Gulf. Hydrodynamics (current flows, sea level and waves) within the Firth are strongly linked to large-scale oceanographic and meteorological processes occurring within the wider Hauraki Gulf (Black et al. 2000; Bell et al. 2004), but also have a locally-generated component within the Firth driven by local winds and catchment runoff. For example, storm surges and tides in the Firth are influenced by the wider Hauraki Gulf (and beyond), whereas surface drift and waves in the southern Firth are more influenced by local winds and river flows. These hydrodynamic processes in turn affect sediment transport and mangrove-propagule dispersal.

Rapid mangrove-habitat expansion in the Firth of Thames and other North-Island estuaries raises a number of questions that are relevant to the long-term fate of mangrove systems and estuaries. Firstly, what has triggered mangrove-habitat expansion decades after deforestation? Secondly, how are mangroves altering estuaries? Lastly, what is the long-term fate of these mangrove habitats given the potential effects of climate change?

1.2 Role of mangroves in coastal-hazards mitigation

Low-lying coasts can be vulnerable to erosion and inundation by waves, tides, storm surge and tsunami. Mangrove forests growing on intertidal areas may mitigate the adverse effects of these coastal hazards. Mangroves effectively dampen tidal currents (Furukawa et al. 1997) and attenuate sea and swell waves, due to drag, as they propagate through the network of pneumatophores, trunks and canopy on the mangrove fringe, and in doing so protect the backshore from direct wave attack and erosion (Othman, 1994; Brinkman et al. 1997; Massel et al. 1999; Phuoc & Massel, 2006). In tropical environments, mangrove forests may also substantially reduce the damage caused by cyclones and tsunamis (Dahdouh-Guebas et al. 2005). In New Zealand, the potential role of mangrove in coastal-hazards mitigation has not previously been considered. The low-lying coast of the southern Firth of Thames is potentially exposed to erosion and inundation due to sea and swell waves, storm surge and tsunami. The contribution of mangroves to coastal hazards mitigation in the southern Firth is considered in the present study.

1.3 Study objectives

Environment Waikato commissioned NIWA to undertake a study of mangrove-habitat expansion and sedimentation processes in the southern Firth. The main objectives of the study are to:

- Reconstruct the historical sequence mangrove-habitat expansion based on historical aerial photography (1944–2005) and dated sediment cores.
- Quantify sediment accumulation rates (SAR) and changes in SAR resulting from mangrove colonisation and habitat expansion.
- Determine the role of mangrove habitat in mitigating coastal erosion and inundation hazards in the southern Firth. This assessment includes consideration of shoreline erosion by waves and coastal inundation due to tides, storm surge, tsunami and the potential future effects of sea-level rise based on historical trends the latest IPCC (2007) projections.

1.4 Report outline

Section two describes the Firth of Thames study area including estuarine processes and catchment history. Section three provides details of the methods used in the study. Results are presented in section four. In section five this new information is used to: (1) reconstruct the sequence of mangrove-habitat expansion; (2) identify triggers and controls, environmental effects; (3) predict the long-term fate of the mangrove forest; and (4) assess the role of the mangrove forest in coastal hazards mitigation in the southern Firth of Thames.

2. Study area and hazards

2.1 Physical setting

The Firth of Thames is a 800 km² meso-tidal¹ estuarine embayment on the east-coast of the North Island (37°S 175.4°E) 70-km south-east of Auckland (Fig. 1.1). The Firth occupies the Hauraki Depression, which is a structural graben (Healy, 2002) bounded to the east and west by the Coromandel and Hunua Ranges respectively. To the south are the low-lying Hauraki Plains, which are underlain by estuarine sediments (Woodroffe et al. 1983). The Firth receives runoff from a 3600 km² catchment and primarily from the Waihou (1966 km²) and Piako (1476 km²) Rivers, which deliver an estimated 150,000 t yr⁻¹ and 35,000 t yr⁻¹ of suspended sediment respectively (Hicks and Shanker, 2004). The Waihou River has delivered sediment to the Firth for the last 20,000 years or so. Shoreline-progradation rates have averaged 1.7 m yr⁻¹ over the last 6,500 years (Hochstein and Nixon, 1979; de Lange and Lowe, 1990) and a chenier plain has formed in the last *c.* 3,600 years along the western shore of the Firth (Woodroffe et al. 1983).

2.2 History

Pre-human catchment landcover consisted of podocarp–hardwood forests on the Coromandel and Hunua ranges. The Hauraki Plains were occupied by freshwater marshes and swamp forests dominated by Kahikatea (*Dacrydium dacrydioides*). Early Maori arrived *c.* 1,000 years ago and settled the higher levee along the banks of Waihou and Piako Rivers. Forest clearance was mainly restricted to the immediate areas around settlements (Phillips, 2000). European settlers arrived in the mid-1800s and large-scale deforestation began shortly after in the Coromandel ranges, which was associated with timber logging and gold-mining (Brownell, 2004). These activities substantially increased sediment loads to the Firth. Hydrographic surveys conducted by the Public Works Department in 1882 and 1918 indicate that *c.* 7 x 10⁶ m³ of sediment was deposited within a 16 km² area of the lower Waihou River and its tidal delta (Fig. 1.1) and an estimated 37 x 10⁶ m³ was deposited in a 210 km² area of the Firth south of Tararu. The conversion of the Hauraki Plains to pastoral agriculture was delayed until drainage works began in 1905. A stopbank was constructed along the southern shore of the Firth and the tidal reaches of the Waihou and Piako Rivers. By 1920 some 162 km² of swamp had been converted to pasture (Brownell, 2004). The 1938 storm flooded the entire Hauraki Plains and consequently the height of the

¹ *Meso-tidal* refers to a classification of coastal environments where the tidal influence is strong, but not necessarily dominant, and usually have a moderate tide range of 2–4 m.

stop banks was increased. These engineering works constrained floodwaters to the river channels and are likely to have increased sediment delivery to the Firth.

2.3 Hydrodynamic setting

2.3.1 Depths and mean level of the sea

The Firth progressively shoals from a maximum depth of 35 m at its northern inlet, near Waiheke Island, to the extensive intertidal flats of the southern Firth. The embayment is roughly rectangular in shape being on average *c.* 20 km wide and 55 km long, with its long-axis orientated north–south. Over the past two years (2004–2006), the mean level of the sea² in the Firth is currently around 0.1 m above the local Moturiki Vertical Datum–1953 (denoted MSL in this report). The historical rate of relative sea level rise at the Port of Auckland (1899–2005) has averaged 1.4 mm yr⁻¹ based on the results of Hannah (2004) up to 1999 and extended to include years 2000–2005.

Sea level has been rising in the southern Firth of Thames at a similar rate to Auckland, based on a comparison with the short 1993–2006 sea level record at Tararu (Bell and Goodhue, 2007).

2.3.2 Tides, currents and waves

Tides in the Firth are semi-diurnal, with average spring and neap tidal ranges of 2.9 m and 2.2 m respectively. The highest astronomical tide is *c.* +2.1 m MSL. Tidal currents within the Firth of Thames are typically $\leq 0.3 \text{ m s}^{-1}$ on an average tide (Black et al. 2000). Substantial currents can be generated by regional winds, particularly in the surface layer. Persistent winds from the north to east cause a clock-wise residual circulation, while the prevailing winds from the south and west produce an anti-clockwise circulation (Greig and Proctor, 1989; Bell et al. 2003). The Firth's estuarine-like circulation and residual currents trap river-borne suspended sediments that are deposited in the Firth (Healy, 2002). The integrated long-term (30-year) wind residual pattern is clockwise and directed from east to west along the southern flank of the Firth, for all strong wind events above 15 m s^{-1} (Bell et al. 2003). These conditions are likely to drive substantial mud resuspension and transport by waves and currents. Silt-laden river plumes have also built deltas at the river mouths and adjacent intertidal flats.

² Note: the mean level of the sea (MLOS) is the actual average sea level which varies from year to year and is also increasing due to global warming. Not to be confused with mean sea-level datum (MSL) which is a fixed survey datum across a region.

Northerly winds generate short-period waves, mostly less than 10 second periods and typically < 1 m high. Gorman & Heydenrych (2004) developed a 20-year wave-climate hindcast for the Firth (1979 to 1998). Table 2.1 presents the results of this wave-climate hindcast for Kaiaua (western Firth) and the central Firth. Extreme significant wave heights are seldom > 1.5 m. Wave heights are likely to be attenuated in the southern Firth due to bed friction as the waves propagate over the intertidal mud flats. Wave periods indicate the sea state is mostly local wind-sea, with occasional penetration of swell from the Hauraki Gulf during large cyclonic storms. Swell attenuation will be more pronounced due to the longer wave length so that shoaling will occur in deeper water.

Table 2.1: Firth of Thames 20-year wave-climate hindcast statistics, where H_{sig} is significant wave height, T_{peak} is the period of the peak wave energy and T_m is the average wave period. Wave direction is that from which the predominant wave energy arrives in descending order (source: Gorman & Heydenrych, 2004).

Site	Mean H_{sig} (m)	Max H_{sig} (m)	Mean T_{peak} (s)	Max T_m (s)	Direction
Kaiaua [5 m depth]	0.26	1.25	4.3	8.5	N, NNE
Central Firth [9.7 m depth]	0.41	1.49	5.3	8.6	NNW, N

2.4 Sedimentary setting

The combination of a large tidal range, wind-driven circulation and waves, gently-sloping bed ($< 0.03^\circ$) and large quantities of fine-sediment supplied by catchment erosion has built some 70 km² of intertidal-mud flats in the southern Firth (Fig. 1.1). Mud-flat morphology is similar to that described for the muddy coast of Surinam, South America (Augustinus, 1980; Wells and Colman, 1981). The lower-intertidal flat in the Firth is characterized by fluid-mud deposits, while a “mud bastion” morphology of isolated consolidated-mud mounds ≤ 20 cm high develops on the middle-upper intertidal flat above 0.7 m MSL (Fig. 2.1). On the Surinam coast, these features have been interpreted as remnants of an eroded mudflat (Augustinus, 1980). Above 0.8 m MSL, the mud bastions are replaced by a 300-m wide band of large-scale “mud forms” that resemble an irregular ridge-runnel system (Fig. 2.2). These shore-normal, often bifurcating ridges, are ≤ 0.25 m high with wavelengths ≤ 2 m and sinuous crests up to 50 m long. These features represent large-scale bedforms and similar bedforms are reported by Augustinus (1980) from Surinam’s muddy coast. This intertidal morphology is characteristic of a mesotidal, moderately wave-exposed, muddy coast, with large mud supply, high suspended sediment concentrations (SSC) and rapid

sedimentation. In similar muddy-coast environments, near-bed SSC in the range 10^3 – 10^4 mg l⁻¹ increase fluid density sufficiently to attenuate shoaling waves (Wells and Coleman, 1981, Mehta, 2002).



Figure 2.1: Mud-bastion morphology characteristic of the middle-intertidal flat. Photo taken *c.* 800 m north of mangrove-forest fringe, Transect B (14 March 2006). For scale, mud bastions *c.* 10-cm high.



Figure 2.2: Ridge and runnel bedform morphology developed on the mud flat immediately seaward of the mangrove fringe, Appletree Transect (30 March 2006). Note mangrove tree bottom right of photo. For scale, mudforms are *c.* 30-cm high and the runnels are 1–2 m apart.

2.5 Tectonic setting and tsunami hazard

The Firth of Thames is located within the longer Hauraki Depression, which is recognised as a back-arc rift (Hochstein & Nixon, 1979). North-south trending faults

are associated with this structure and are known to be active. Transverse faults across the Hauraki lowlands cause horizontal offsets of these major faults. The rift structure is infilled with soft Tertiary and weakly consolidated Quaternary sediments to a maximum thickness of about 3 km (de Lange and Lowe, 1990). Onshore, the land slopes up gently towards the south, reaching an elevation of +3 m MSL some 25 km inland.

The best known active geological structure within the Hauraki Rift is the Kerepehi fault, with the submarine section comprising a NNW-striking normal fault located down the central axis of the Firth of Thames (Chick et al. 2001). The offshore section is broken into 4 main segments as shown in Figure 2.3. The predicted moment magnitudes range from 6.5–7.1 and the recurrence interval is estimated to be 2,500 to 4,500+ years (Chick et al. 2001). Although tsunami generation normally requires $M_w > 7.3$ there are known instances where a tsunami has been generated by smaller magnitude earthquakes, particularly if the rupture occurs in soft sediments or the rupture arise from a “slow earthquake”. Further, tsunami-like waves can also be generated within a semi-enclosed basin like the Firth when differential tectonic movement occurs and the water volume has to adjust to the new bathymetry within the basin, as occurred in Wellington Harbour during the 1855 earthquake event.

Consequently, there is a local-source tsunami hazard arising from a potential rupture of the Kerepehi Fault although no historic event has been observed (de Lange & Healy, 2001). Preliminary modelling of the tsunami hazard from the southern-most submarine section of the Kerepehi Fault (A in Figure 2.3) suggest the maximum tsunami run-up height would be in the range 1–1.8 m (Chick et al. 2001). Because of the north-south orientation of the fault in section A, a tsunami generated on this section would likely to have most impact on the eastern and western shores rather than the southern flank.

Other regional (i.e., 1–3 hours travel time) and remote (> 3 hours travel time) sources of tsunami for the Hauraki Gulf are described by de Lange & Healy (2001). The highest vertical run-up heights observed from the 12 historic events analysed since 1840 were 1.8 m at the Port of Auckland (Krakatau eruption, 1883) and 1.5 m in the Tamaki Estuary (northern Chile earthquake, 1868). All historic tsunami events with >1 m runup height were derived from remote tsunami sources. The only documented historic observations of tsunami in the southern Firth were:

- maximum 0.9 m high bore in the Thames area on the 11th May following the 1877 Chile earthquake;

- maximum 1.5 m run-up height at Thames on the 28th August 1883, following the Karatau eruption in Indonesia, where the tide became full during an ebbing flow.

There is also evidence of pre-historic tsunami events in the Auckland region from geological and sedimentological signatures (GeoEnvironmental Consultants, 2005). The two most significant pre-historic events are dated to the late 14th and early 15th century with maximum runup heights in the Auckland region of 14 m and < 10 m respectively. Their sources are most likely to have been outside the region (e.g., Tonga-Kermadec Trench or to north of NZ) and their magnitude in the Firth of Thames is unknown at this stage.

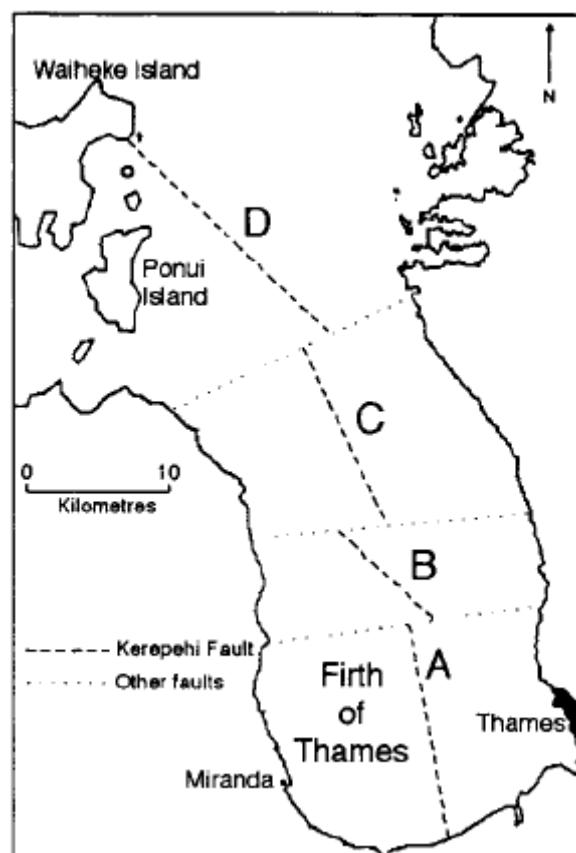


Figure 2.3: Interpreted submarine trace of the Kerepehi Fault (source: Hochstein and Nixon, 1979).

2.6 Storm-tide hazards

Long waves such as the tide and storm surge get amplified as they propagate down the Firth of Thames towards the intertidal mud flats of the southern Firth. For extreme high tides (no wind), the amplification in the high-tide level at Thames is 12–14%

higher than observed at the Port of Auckland. This occurs mainly due to bottom friction as the tides propagate in this shallow embayment. Similarly, storm surge (i.e., long wave of 1–2 days period) is also amplified in the Firth due to bottom friction. Wind set-up will also develop in the southern Firth under northerly wind conditions.

Several historic storm-tide events (i.e., tide and storm surge) have caused coastal erosion and inundation in the southern Firth. The main coastal storm-tide events were:

- **1938:** A storm on 4–5 May 1938 inundated some 35,000 ha of the lower Hauraki Plains (Fig. 2.4). Flooding occurred due to a combination of a perigean-spring tide and north-east gales that caused the storm tide and wave set-up to reach about +3 m MSL on Wednesday evening high tide on 4 May (Ray and Palmer, 1993). As the predicted high tide was +1.74 m MSL (perigean-spring high tide), but with storm surge unlikely to exceed 1 m in New Zealand, the +3 m MSL inundating sea level quoted is likely to have included a component of wave set-up and run-up. The coastal storm caused several breaches of the shoreline stopbank from Waitakaruru to Kopu and Miranda was also damaged by seawater breaking in over the land (Hauraki Plains Gazette, 1938)—again a further indication that wave run-up and overtopping were the main cause of damage. The storm also produced heavy rain from early Wednesday morning which exacerbated the inundation of farmland;



Figure 2.4 : Seawater flooding of the Hauraki Plains in the aftermath of the May 1938 storm. View looking west towards the Waitakaruru River. Piako River in the middle of the photo (source: Hauraki Catchment Board files, Environment Waikato Paeroa office).

- **1978:** several storms hit north-eastern North Island from May to September, causing severe coastal erosion along substantial sections of coast from Northland to the Bay of Plenty. For the Firth of Thames, the main impact was probably from the 19–20 July 1978 storm, when a deep extra-tropical cyclone produced strong north-east to easterly winds that coincided with a perigean-spring high tide of +1.71 m MSL. Storm-surge heights observed at the Port of Auckland peaked at 0.55–0.6 m above predicted high tide for the two high tides on 19 May. Assuming the storm surge was a similar height in the Firth, the storm-tide level would have peaked at 1820 h reaching around +2.3 m MSL in the southern Firth – which matches closely with the observed storm-tide of +2.35 m MSL measured by a tide gauge at the Kopu Bridge (HCBRWB, 1978). The height of waves that were generated in the Firth is unknown, although at the entrance to the Waihou River “heavy wave action” was observed and serious wave damage was done to the stopbank near Turua, upstream from the Kopu Bridge (HCBRWB, 1978).
- **1995:** A storm on 14–15 July, coinciding with very high perigean-spring tides of +1.94 m MSL to give a peak storm-tide level of +2.5 m MSL measured at the Tararu sea-level gauge on the evening of 14 July. This storm-tide along with wave set-up and run-up caused sea inundation of the Moanataiari suburb of Thames, resulting in flooding of over 30 properties (Duder et al. 1999). A Civil Defence Emergency was declared for Thames and Plains Wards with 30 evacuees due to flooding of low lying land by the sea and river flows. The July 1995 storm caused direct damage of \$3 million (2004 values) and 200 insurance claims.
- **1997:** Extra-tropical cyclone *Drena* hit the upper North Island on 11–12 January causing severe damage, including another sea-inundation episode at Moanataiari, Thames (Duder et al. 1999). This storm coincided with a high perigean-spring tide (+1.85 m MSL) to give a storm-tide level of +2.02 m MSL measured by the Tararu sea-level gauge at 0845 h on 11-Jan-1997. High wave activity would have contributed to wave overtopping as the storm-tide level wasn't high relative to other historical events.
- **1999:** A storm on the 17 April caused the storm tide level to reach +2.35 m MSL at 0735 h with heavy wave activity. The newly built seawall at Moanataiari survived this event (Duder et al. 1999).
- **2005:** Severe northerly gales were produced by a deep low (976 hPa) off west of North Island on 18 September 2005 (Election Day). Northerly winds up to 135 km hr⁻¹ were recorded at Cape Colville. Sea inundation occurred at

Thames in the early evening, when the predicted perigean-spring high tide of +1.78 m MSL was elevated by the inverted barometer effect and wind set-up to register a storm-tide of +2.33 m MSL measured by the Tararu gauge.

3. Methodology

3.1 Mangrove-habitat expansion

The historical sequence of mangrove-habitat expansion in the southern Firth of Thames was reconstructed from vertical-aerial photography collected over the last 60 years. Aerial photographic coverage of the southern Firth is available for the years 1944, 1952, 1963, 1977, 1987, 1996, 2002 and 2006. The images were digitised and geo-referenced by the Resource Information Group, Environment Waikato. Contact prints of the 1944–1996 images were scanned into either JPEG or TIFF file formats. These digitised images were merged to build mosaics using Photoshop software and geo-referenced using the Intergraph Geomedia GIS software. An affine transformation was used to transform points in the raster images and reference to ground control points. The 2002 and 2006 images were supplied to Environment Waikato as GIS-ready ortho-imagery by Terralink International Limited. All other aerial photographs were supplied by Environment Waikato from various sources (copyright reserved). The Intergraph Geomedia software was also used to merge the aerial photography with the locations of sediment cores and shore-normal elevation profiles.

3.2 Shore-normal elevation profiles

Shore-normal elevation profiles were measured through the mangrove forest to:

- provide information on large-scale coastal morphology;
- relate bed elevations within the mangrove forest and mudflat to mean-sea level (MSL or Moturiki Vertical Datum-1953);
- relate dated sediment cores collected within the mangrove forest and mudflat to mean-sea level (MSL, Moturiki 1953) datum;
- provide information for the coastal erosion and inundation hazards assessment.

The elevation profiles were surveyed during 25–28 January 2005 along three shore-normal transects (A–C) at *c.* 2-km intervals alongshore and up to 1200-m seaward of the flood-defence stopbank landward of the mangrove forest (Fig. 1.1). Elevations were measured to ± 0.5 cm using a Geodimeter Model 464 total station. The seaward half of Transect C could not be surveyed because of difficulty in accessing the site. The locations of the profiles were selected based on analysis of the historical aerial

photographs. The photographs indicate that initial mangrove colonisation and habitat expansion over the last 50 years or so has occurred relatively uniformly along the coast.

3.3 Sedimentation

The recent sedimentation history of the southern Firth was reconstructed using dated sediment cores collected from the present-day mangrove forest and mud flat. The sediment cores record the physical conditions that prevailed on the mud flats before, during and after mangrove colonisation and habitat expansion. The oldest sediments sampled in the cores date back to the late 1800s. These cores preserve evidence of how mud deposition and mangrove-habitat expansion has resulted in large-scale environmental changes in the southern Firth of Thames.

Sediment cores were collected along Transect B (i.e., Appletree), which is located mid-way between the Waitakaruru and Piako Rivers (Fig. 3.1). Transect B was selected for coring because sediments deposited here should preserve changes in physical conditions on the mud flats that are representative of the Southern Firth in general. Closer to the river mouths, sedimentation is also likely to be influenced by local effects, such as deltaic and levee sedimentation, bar and channel migration associated with the river plumes.

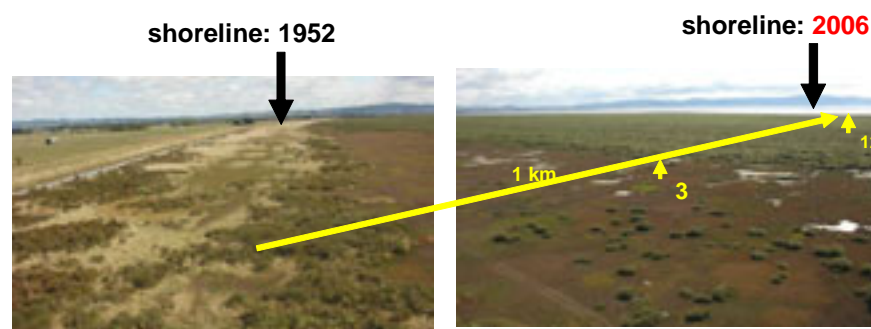


Figure 3.1: View of Transect B looking west. The location of the transect is indicated by the yellow line. Core site 3 is close to the landward edge of the mangrove forest and site 12 is located *c.* 50 m seaward of the seaward edge of the mangrove. Glasswort (*Sarcocornia quinqueflora*) saltmarsh occupies a 200-m wide zone between the mangrove forest and an area of saltmarsh ribbon wood (*Plagianthus divaricatus* J.R. Forst. & G. Forst) and *Muehlenbeckia complexa* (A. Cunn.) Messn (scub pohuehue) with tall fescue grass (*Schedonorus phoenix* (Scop.) Holub) adjacent to the stopbank (identification: Dr Catherine Beard, Environment Waikato).

Replicate sediment cores 7.5-cm-diameter and ≤ 1.9 -m long were collected during 22–24 February 2005 from the mangrove forest along Transect B (February 2005) using a Livingston piston corer (Table 3.1, Fig. 3.2, **LC sites** 3–11). A 0.7-m-long push core (site LC-12) was collected from the mud flat 50-m seaward of the mangrove-forest fringe. Replicate short cores 40-cm long and 10-cm diameter were also collected at sites LC-3 – LC-11. These cores were intended to provide large samples, and thereby minimise measurement uncertainties, for radioisotope dating of near-surface sediments. Radioisotope concentrations are highest and decline most rapidly near the surface. Figure 3.2 shows the location of the sediment cores along Transect B.

Sediment core were not collected at sites one and two as originally planned. Site one was located within the area of saltmarsh ribbon wood near the landward end of Transect B. Site two (distance 185 m, Fig 3.2) was located in the glasswort (*Sarcocornia quinqueflora*) saltmarsh. Coring was attempted at site two but was unsuccessful due to the high water content of the sediment.

Table 3.1: Sediment core locations along Transect B collected from the mangrove forest (LC-3 to LC-10) and mud flat (LC-11 and LC-12). Distance is relative to total station position on top of stopbank. Elevation is in metres above mean sea level (MSL).

Core site	Distance (m)	Elevation (m MSL)	NZMG East	NZMG North
LC-3	305	1.74	2727954	6440321
LC-4	400	1.74	2727558	6440421
LC-5	501	1.81	2727524	6440513
LC-6	565	1.84	2727503	6440573
LC-7	634	1.77	2727478	6440637
LC-8	726	1.72	2727447	6440723
LC-9	814	1.71	-	-
LC-10	902	1.17	2727388	6440888
LC-11	930	0.92	2727380	6440915
LC-12	978	0.97	-	-

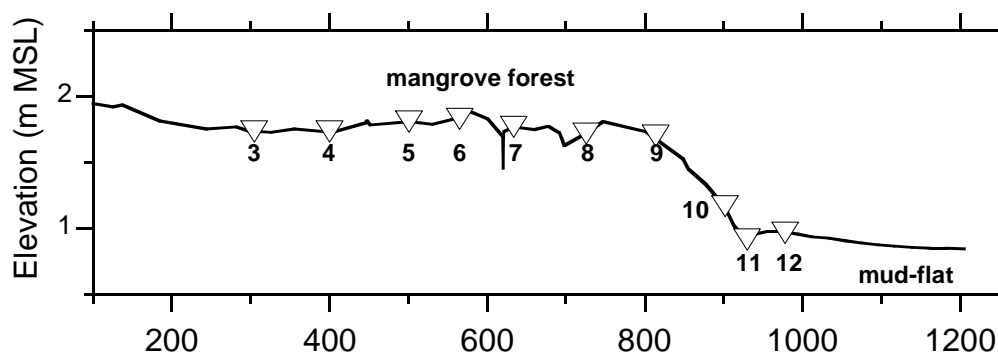


Figure 3.2: Sediment-cores locations along Transect B (LC-3 – LC-12). The mangrove-forest fringe (seaward edge) was at site LC-11 in February 2005. Bed elevations are relative to mean sea level Moturiki Vertical Datum 1953.

The cores were logged and sub-sampled at depth intervals in 2-cm-thick slices for radioisotope and pollen dating, and bulk density and particle-size determination. Core-compression was < 5% at all sites.

3.3.1 Sediment dating

The sediment cores were dated using radioisotope and pollen techniques. Radioisotopes, such as caesium-137 (^{137}Cs , $t_{1/2}$ 30 years) and lead-210 (^{210}Pb , $t_{1/2}$ 22.3 years), and plant pollen can be used to reconstruct the recent sedimentation history of an estuary.

Sediment accumulation rates (SAR) were estimated from lead-210 (^{210}Pb , $t_{1/2}$ 22.3 yr) and caesium-137 (^{137}Cs , $t_{1/2}$ 30 yr). Concentrations of the cosmogenic radioisotope beryllium-7 (^7Be , $t_{1/2}$ 53 days) were also measured in the core samples. ^7Be is particle reactive and tends to be concentrated in aquatic systems, making it a useful sediment tracer in fluvial-marine systems at seasonal timescales (Sommerfield et al. 1999). In the present study, ^7Be is used to provide information on the depth and intensity of sediment mixing. The radioisotope-dating techniques used in the present study are described in Appendix One.

Radioisotope activity concentrations expressed in S.I. units of Becquerel (disintegration s^{-1}) per kilogram (Bq kg^{-1}) were determined by gamma-spectrometry. For simplicity, we will refer to the activity concentrations of ^{137}Cs and ^{210}Pb as concentrations. Dry samples (40–60 g) were counted for 23 hrs using a Canberra Model BE5030 hyper-pure germanium detector. The unsupported or excess ^{210}Pb concentration ($^{210}\text{Pb}_{\text{us}}$) was determined from the ^{226}Ra ($t_{1/2}$ 1622 yr) assay after a 30-day ingrowth period for ^{222}Rn ($t_{1/2}$ 3.8 days) gas in samples embedded in epoxy resin.

Gamma spectra of ^{226}Ra , ^{210}Pb and ^{137}Cs were analysed using Genie2000 software. The radioisotope data for the long and short cores collected at sites LC-3 – LC-11 were combined for analysis.

The $^{210}\text{Pb}_{\text{us}}$ profiles in each core were used to determine: (1) time-averaged SAR from regression analysis of natural log-transformed data; (2) $^{210}\text{Pb}_{\text{us}}$ inventory (A , Bq cm^{-2}) and; (3) mean annual supply rate (P , $\text{Bq cm}^{-2} \text{ yr}^{-1}$) based on the ^{210}Pb decay coefficient (k , 0.0311 yr^{-1}). These data were compared with the ^{210}Pb atmospheric flux ($0.005 \text{ Bq cm}^{-2} \text{ yr}^{-1}$) measured by NIWA at Auckland. SAR were estimated from ^{137}Cs profiles based on the maximum depth of ^{137}Cs in each core and included corrections for sediment mixing indicated by ^7Be profiles. In NZ, ^{137}Cs deposition from the atmosphere was first detected in 1953 (Matthews, 1989).

Pollen dating was attempted for long cores LC-3 to LC-12 taken from the mangrove forest and adjacent mudflat. Sediment sub-samples of 1–2 cm^3 volume were taken from each core at *c.* 10-cm depth intervals. Samples were prepared for pollen analysis by the standard acetylation and hydrofluoric acid method (Moore et al. 1991). Fern and other plant spores are included as pollen types. The pollen sum, that is the number of pollen grains counted per sample, was at least 300 grains. This sum excludes wetland taxa and ferns except bracken (*Pteridium esculentum*), and marine dinoflagellates. Following convention, certain taxa are excluded from the base count for graphing purposes, but are still expressed as a percentage of the pollen sum total; sample totals may therefore exceed 100% in the pollen diagrams.

Wetland taxa and ferns are usually excluded because they tend to have highly fluctuating pollen and spore production which distorts percentages. However, in New Zealand pollen studies, bracken fern is often included in the pollen sum because it may form a substantial proportion of the land vegetation cover. Fragmented pollen grains and spores were counted as individuals. The undifferentiated (undif) conifers category includes all conifers (native and introduced) except *Cupressaceae* (the cypress family) and kauri (*Agathis australis*). These pollen types were often difficult to differentiate because of fragmentation. The pollen profiles in the sediment cores for the major plant groups are expressed as a percentage of the terrestrial pollen sum. Appendix One describes pollen dating in more detail.

3.3.2 X-radiographs

An x-ray image or x-radiograph provides information on the fine-scale sedimentary fabric of deposits. For example, density differences between thin laminae of silt and sand or animal borrows that are infilled with mud make these subtle features may not be visible to the naked eye.

X-radiographs were taken before the cores were logged and sub-sampled. Sediment fabric was determined from x-radiographs prior to sub-sampling. The long cores were split and sectioned into 40-cm long and 2-cm-thick longitudinal slabs and imaged using a Phillips Model Macrotank 205 X-ray generator with Kodak AA400 film (50 kV, 5 mA, 1.1 min). The x-rays films were digitised as follows. Films were illuminated using a Kaiser Prolite 5000 high-frequency 5000°K lightbox. A Nikon D1x digital SLR camera with 60mm f2.8D microNikkor lens (ISO 125, f6.3 or f7.1 aperture) was used to image the films. File format is black and white RGB-tif files with 3008 x 1960 pixels. The images were cropped and in some cases duplicated and image and contrast adjustments made using the Adobe Photoshop software.

3.3.3 Sediment bulk density

Sediment wet- and dry-bulk densities were determined for sediment samples prepared for radioisotope analysis. Typically $\frac{3}{4}$ of the 2-cm thick slices from the sediment core were sampled. The samples were weighed on a chemical balance to the nearest 0.01 g then dried at 70°C for 24 hours and re-weighed to obtain the dry-sample weight. The sediment bulk densities were calculated from the wet and dry-sample weights and the sample volume.

3.3.4 Particle-size analysis

Particle-size distribution (PSD) was determined using a Galai CIS-100 “time-of-transition” (TOT) stream-scanning laser particle sizer. Sediment samples were wet-sieved through a 2-mm sieve to remove vegetation fragments and shell hash. The sediment was homogenised in a one-litre suspension and a sub-sampled using an auto-pipette. Samples were also dispersed in an ultra-sonic bath for 10 minutes before and during particle-size analysis. The PSD was determined in the ranges 0.5–300 μm and 2–600 μm as required, with typically *c.* 500,000 particles measured per sample. Particle volumes based on spheres were estimated from the measured particle diameters. These data were used to construct volume-based PSD.

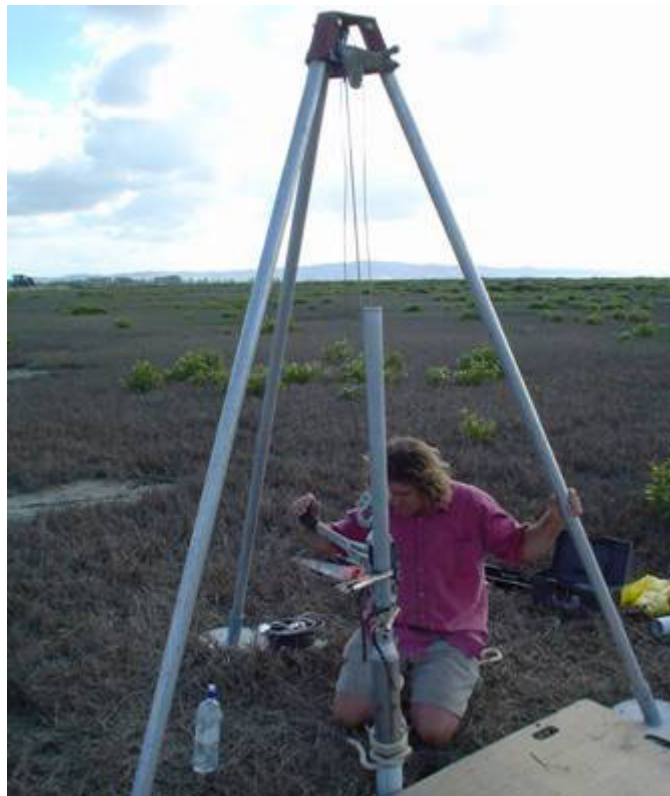


Figure 3.2: Sediment coring at site LC-2. Cores are collected in PVC pipe using a Livingston piston corer. The core is extracted from the sediment column using a winch.

3.4 Tides and storm surge

The tide gauge at Tararu (37.133°S, 175.542°E) located 3 km north of Thames provides a sea level record for the southern Firth (Site #9415, 1 Nov. 1992– present). The sea-level record for the period 2004–2006 was analysed to determine: (1) the duration of tidal inundation (2004–2006) of the mangrove forest; and (2) exceedance probability (%) for predicted high-tide levels (1900–1999 AD). The inundation time for specified vertical levels was determined for predicted tides, using tidal constituents for 2004–2006, and measured storm tides. This recent period is representative of the tide and storm surge conditions that influence the **present-day** mangrove forest. The mean level of the sea during 2004–2006 has been around 0.11 m above the local Moturiki Vertical Datum–1953 (MVD-53). We subsequently refer to MVD-53 as the mean sea level (MSL) datum.

The predicted high tide levels for the period 1900–1999 used to determine the exceedance probability (%) of upper tide levels is determined for several summary parameters. Mean high water spring (MHWS), using the nautical definition of adding the M_2 and S_2 tidal amplitudes, is +1.6 m MSL and is exceeded by 23% of all high

tides based on a 100-year set of tide predictions. The higher mean high water perigean-spring tide (MHWPS) occurs when spring tides coincide with the moon's perigee. The MHWPS tide is 1.87 m above MVD-53 and is exceeded by only 5% of all high tides. The highest astronomical tide is +2.08 m MSL.

An algorithm was applied to the sea-level record to determine the percentage of time that a specified level on the mudflat is inundated by the tide during the period 2004–2006. Gaps in the record were excluded and spikes were replaced by interpolated values from adjacent measurements. The time in hours and the percentage of the time that a series of specified vertical levels are inundated, was determined for both the predicted tides only (using tidal constituents derived for the two-year period) and for the actual storm-tide measurements from the sea-level gauge.

4. Results

4.1 Mangrove-habitat expansion in the southern Firth

The historical aerial photographs document mangrove colonisation and habitat expansion that has occurred in the southern Firth. Mangrove stands were restricted to delta deposits flanking the river mouths in the mid-1940s (Figs. 4.1 and 4.2). The 1944 coverage does not include the coast west of Transect B (Appletree). At this time, saltmarsh occupied the upper-intertidal zone along the coast between the Piako and Waitakaruru Rivers. The 1952 photographs show that the mangrove distribution had not substantially changed since the mid-1940s. At Waitakaruru, mangrove was present on the upper-intertidal flats up to 1.5 km east of the river mouth.

By 1963, mangrove had colonised along the entire coast between the river mouths and by that time, and were present at Transect B on the middle-intertidal flat 300 m seaward of the stopbank. The mangrove stand at this time was *c.* 50 m wide and *c.* 10 metres seaward of core site LC-3 (Fig 4.3a). The 1944–1963 photo sequence also clearly show that saltmarsh habitat was progressively colonising the upper-intertidal flat.

By 1977 mangrove forest had spread seaward, and landward to a more limited extent, and occupied a 500-m wide zone along the entire coast of the southern Firth. The 1977 aerial photograph indicates that the density of mangrove forest cover varied alongshore, being highest near the river mouths. At Transect B the mangrove-forest fringe was located at core site LC-6. Figure 4.4 is a photograph of the intertidal flats *c.* 200 m west of Transect B that was taken sometime during the period 1972–1974 by a local resident.

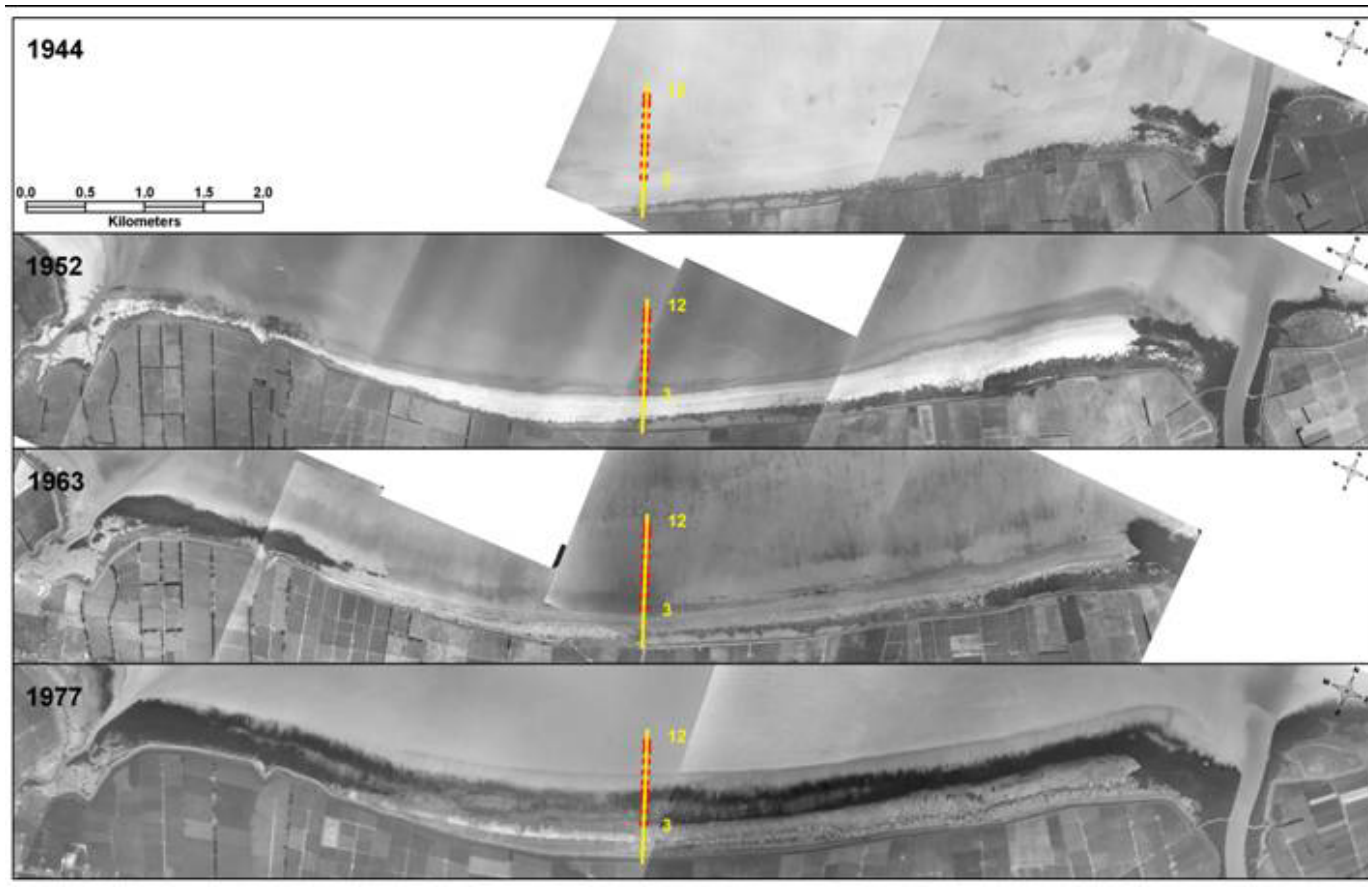


Figure 4.1: Southern Firth of Thames shoreline between Waitakaruru and Piako River mouths. Aerial photo-mosaics for 1944, 1952, 1963 and 1977. The location of Transect B (yellow line) and core sites LC-3 to LC-12 (red circles) are shown.

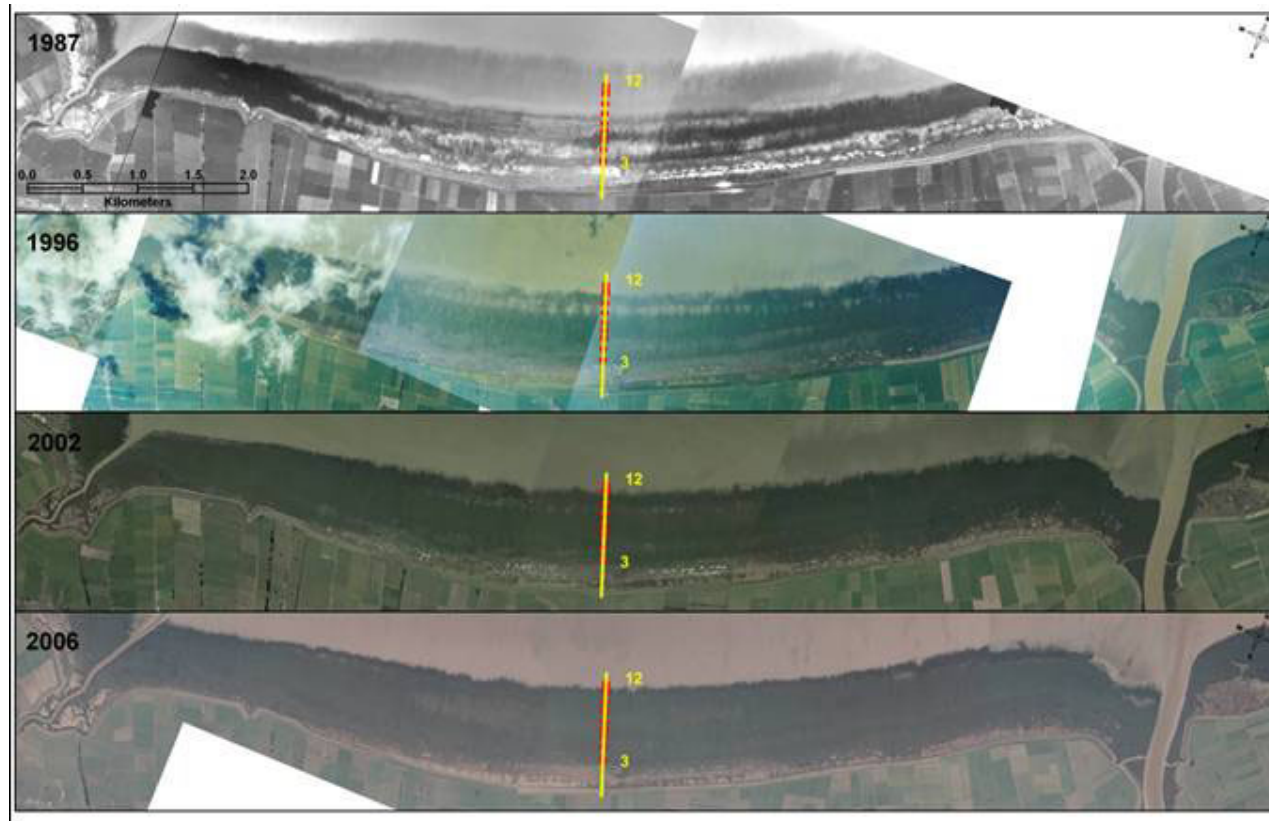


Figure 4.2: Southern Firth of Thames shoreline between Waitakaruru and Piako River mouths. Aerial photo-mosaics for 1987, 1996, 2002 and 2006. The location of Transect B (yellow line) and core sites LC-3 to LC-12 (red circles) are shown.

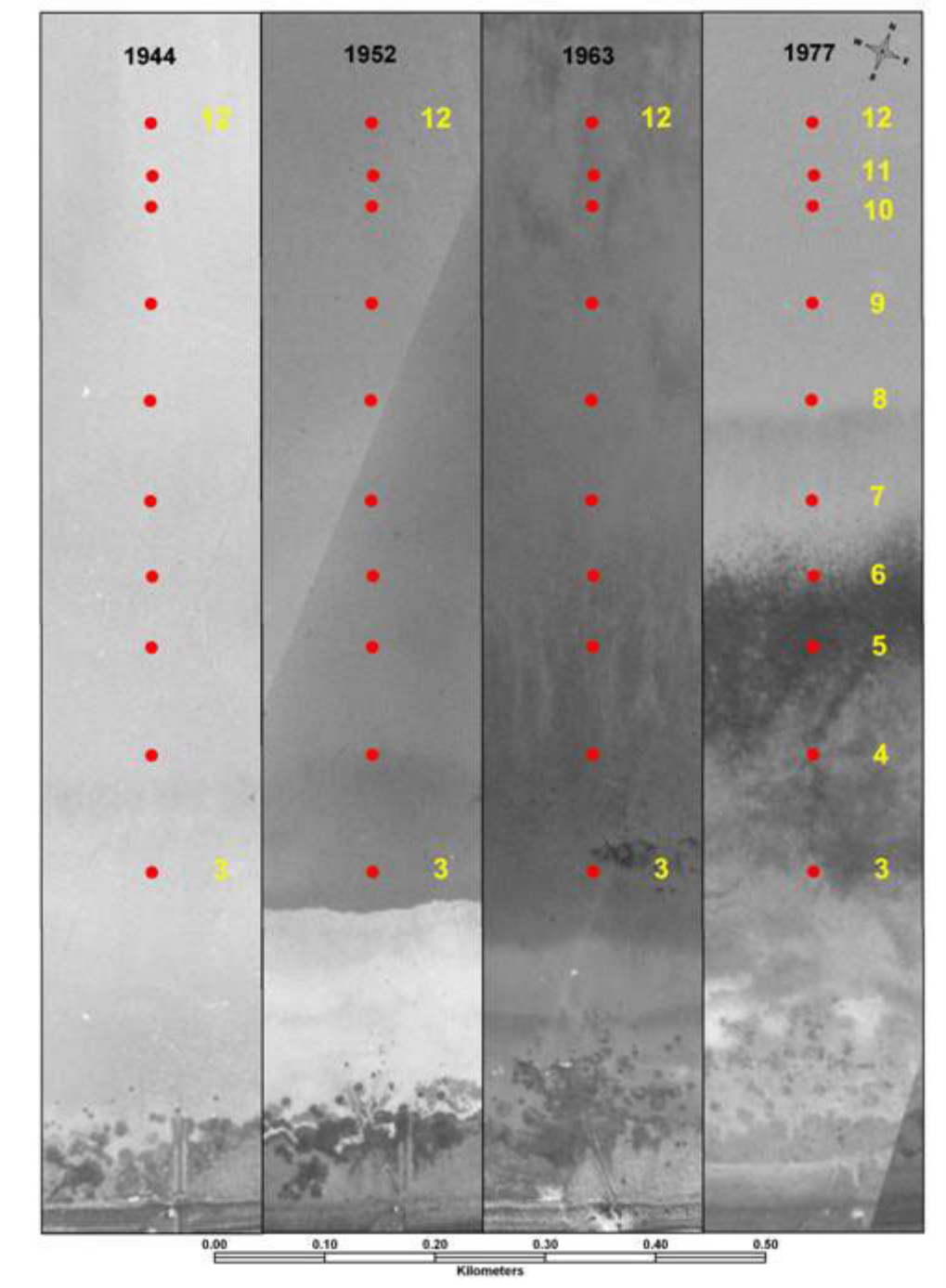


Figure 4.3a: Transect B (Appletree): aerial photographs of the intertidal flat ± 100 metres east and west of the transect: 1944, 1952, 1963 and 1977. The locations of the sediment cores (sites 3–12) collected in 2005 are also shown.

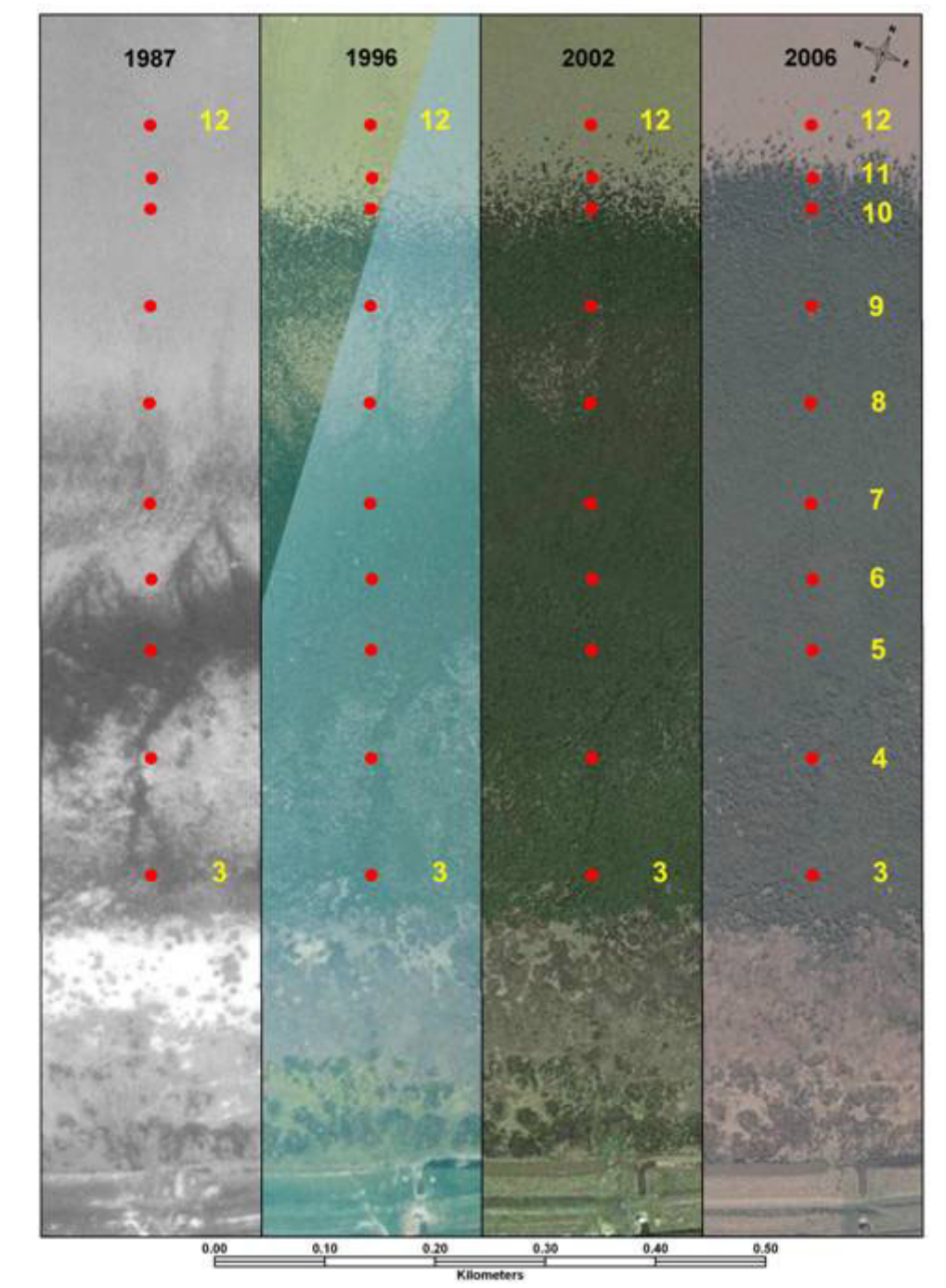


Figure 4.3b: Transect B (Appletree): aerial photographs of the intertidal flat ± 100 metres east and west of the transect: 1987, 1996, 2002 and 2006. The locations of the sediment cores (sites 3–12) collected in 2005 are also shown.



Figure 4.4: Transect B (Appletree) in the early 1970s. View of the intertidal flat with mangrove present. Photo provided by Mrs Allyson McAulay (local farmer).

Figure 4.3b shows that the mangrove forest has continued to spread seaward since the 1970's. By 2002 the mangrove forest occupied a c. 800-m wide zone and c. 7 km² of former intertidal flat between the Waitakaruru and Piako Rivers.

We distinguish between **old-growth mangrove forest** that colonised the mudflats before the mid-1970s and more **recent mangrove forest** that has established since that time. The geographic boundary for these forests occurs between core sites LC-5 and LC-6. Figure 4.3a shows that LC-6 was located on the seaward fringe of the forest in 1977. The distinction between old and recent mangrove forest is based on major differences in forest development and sedimentation histories (sections 4 and 5).

The aerial photographs indicate **at least four major mangrove seedling recruitment events** have occurred since the early-1950s and during the time intervals:

- 1952–1963
- 1963–1977
- 1977–1987
- 1987–1996

The photographs also show that the mangrove-forest has not substantially increased its seaward extent since 1996, implying that no major seedling recruitment has occurred in the last decade (Fig. 4.3b). Seedling recruitment occurs during the summer with propagules settling on the mudflat seaward of the mangrove forest. This propagule-

settling zone is typically several-hundred metres wide (Swales et al. 2007). The timing of mangrove-seedling recruitment events is refined in section five using the dated $^{210}\text{Pb}_{\text{us}}$ profiles.

An interesting feature of the aerial photographs is the apparent loss of mature mangrove forest between 1977 and 1987 (Figs 4.3a and b). For example, core site LC-6 was located on the seaward edge of the mangrove forest in 1977, which appears as a continuous dense cover in the photograph. By 1987, LC-6 was located *c.* 15 m seaward of the forest fringe. Mangrove forest loss occurred along a 3-km section of coast between Transect A (west) and extending *c.* 1-km east of Transect B (Fig. 4.1 and 4.2).

The pattern and scale of the mangrove-forest destruction implies that a natural event occurred during the 1977–1987 period and of sufficient magnitude to damage/remove several hectares of mangrove forest. Evidence for, and the origin of, the event(s) responsible for this mangrove-forest loss are discussed in section five.

4.2 Tides, storm surge and large-scale geomorphology

The tide record for the period October 2004–October 2006 contained gaps of *c.* 5 days. The total elapsed time for this period was 17,389 hours or nearly 725 days. The **highest predicted tide** during the period 2004–2006 was +1.92 MSL, which was slightly higher than the mean high water perigean-spring tide MHWPS level. The highest **measured storm-tide** reached +2.33 m MSL on 18 September 2005, which coincided with a peak storm surge height of 0.5 m. Table 4.1 and Figure 4.5 summarise the results of the tidal-inundation analysis. Below about the mean high water (MHW) mark, the cumulative inundation time is similar for both the predicted and measured storm-tides. This reflects the even balance of negative and positive storm surge in the mid range of tides. As expected, storm-tide events account for an increasing proportion of inundation of the mangrove forest at the upper end of the tidal range.

Table 4.1: Summary of cumulative inundation time of the mangrove forest based on the Tararu sea-level record (Oct-2004–Oct-2006). Definitions: MLOS = mean level of the sea, MHW = mean high water, MHWS = mean high water spring, MHWPS= mean high water perigean-spring tide.

Water Level (m MVD-53)	Tide Level	Predicted Inundation time (%)	Predicted Inundated time (hours)	Measured Inundation Time (%)	Measured Inundation Time (hours)
MLOS	≥0.1	50	8751	50	8756
MHW	≥1.29	10.1	1765	10.4	1813
MHWS	≥1.6	2.1	367	2.5	441
MHWPS	≥1.87	0.10	17	0.35	61
Upper shore	≥2.0	–	–	0.10	17

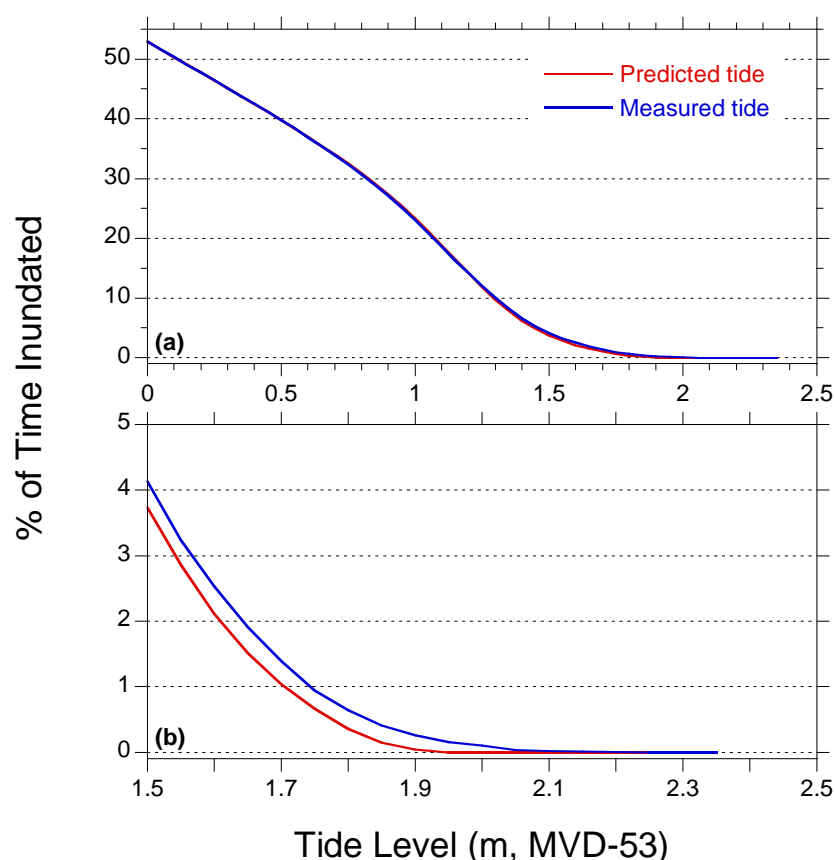


Figure 4.5: Tidal-inundation curves expressed as a percentage of the record (October 2004 – October 2006): (a) all data and (b) tides ≥ 1.5 m MVD-53. Tide level in metres relative to mean sea level (Moturiki vertical datum 1953, MVD-53).

The shore platform that has developed under the mangrove forest at Transects A–C is between MHWPS (+1.87 m MSL) and MHWS (+1.6 m MSL) tide levels (Fig. 4.6). Thus, the mangrove forest today is near the upper limit of the tide and is inundated < 3% of the time. The profiles show a west-to-east elevation trend, with surface elevations at Transect-A being as much as 0.4 m higher than at Transect-C. The elevation difference is most pronounced in the old-growth forest landward of site LC-6. The maximum elevations of the stopbank at Transects A, B and C are +3.74, +3.78 and +3.42 m MSL respectively.

The mud beach under the forest fringe has a convex-upwards shape (Fig. 4.6) that is characteristic of stable or prograding muddy coasts (Mehta, 2002). This prograding beach face slopes seaward at 0.37° and is ten-times steeper than the adjacent mudflat. Mean high water neap tide (MHWN, 0.98m MSL) coincides with the seaward edge of the mangrove forest.

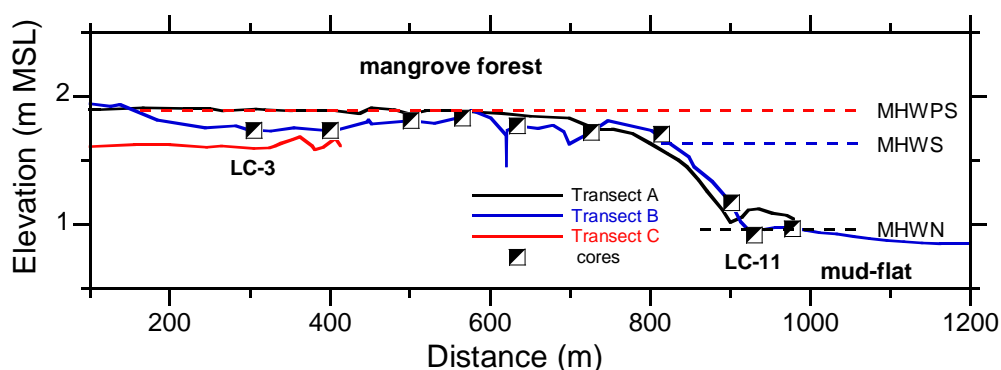


Figure 4.6: Transects A-C shore-normal elevation profiles, January 2005. Surface elevations in terms of mean sea level (Moturiki Vertical datum-1953, MVD-53). Distance is relative to the centre of the stopbank. MHWPS is Mean High Water Perigeon Spring tide at +1.87 m MSL, MHWS (mean high water spring, +1.6 m MSL) and MHWN (mean high water neap, +0.98 m MSL) tides.

The total period of tidal inundation of the mangrove forest rapidly declines with elevation on the forest fringe, from 25% on the mudflat to < 3% on the platform landward of LC-9 (Figs. 4.5 and 4.6). Meteorological or storm tides increase the length of time that the mangrove forest above +1.7 m MSL is flooded by some 40%. At Transect-B this is equivalent to an additional 30 hrs per year of inundation. The largest storm tide measured during 2004–2006 was +2.33 m MSL and occurred on 18 September 2005. This storm tide was 0.6 m higher than the predicted tide.

4.3 Sedimentation

4.3.1 How might mangrove-habitat expansion affect sedimentation?

Mangroves effectively dampen tidal currents (Furukawa et al. 1997) and attenuate waves due to drag as they propagate through the network of pneumatophores, trunks and canopy on the mangrove fringe (section 1.2). Maximum drag-induced wave attenuation will occur when the forest canopy is submerged, which varies with growth stage, water depth and over the spring-neap tidal cycle. Tranquil conditions develop within tens of metres of the mangrove-forest fringe (Furukawa et al. 1997; Janssen-Stelder et al. 2002) so that sedimentation rates are highest here. As the mangrove forest expands across the mudflat, previous fringe areas become old-growth forest that is isolated from the mudflat. Sedimentation rates decline over time in the old-growth forest as surface elevations increase as tidal inundation becomes infrequent and eventually SAR does not exceed the rate of sea level rise (Woodroffe, 2002).

Figure 4.7 shows how the sequence of mudflat colonization by mangrove, subsequent forest development and resulting changes in sediment supply might be preserved in a ^{210}Pb sedimentation record. SAR increase as the mudflat is colonised by mangroves, however this occurs when seedlings have grown in size and/or density sufficiently to influence local hydrodynamic conditions.

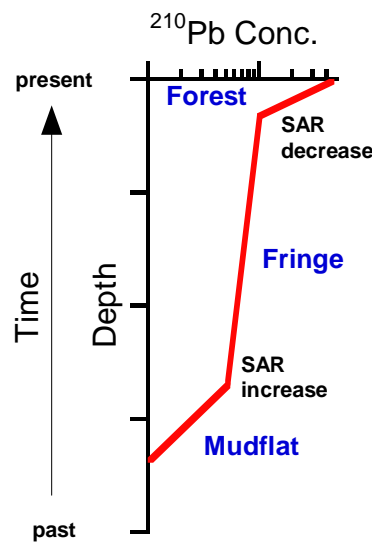


Figure 4.7: Example of a ^{210}Pb **stair-step** profile recording changes in sedimentation rates in a core taken from a mangrove forest that has colonised a former mudflat.

SAR eventually decline as the forest develops and is isolated from the mudflat sediment supply by elevation and distance. The ^{210}Pb profile preserves these changes in sedimentation rate over time as abrupt changes in profile slope. This type of ^{210}Pb profile is known as a **stair-step profile**.

4.3.2 Sediment-core physical parameters

In this section we present interpretations of individual sediment cores based on x-radiographs, particle size, bulk density and radioisotope (dating) profiles from which time-averaged sediment accumulation rates (SAR) and mixing depths are derived. Unsupported ^{210}Pb ($^{210}\text{Pb}_{\text{us}}$) concentration profiles are the basis for estimating ^{210}Pb SAR (Appendix One).

Figure 4.9 presents information on physical sediment characteristics and sediment accumulation rates for core LC-3. This format is used to describe sediment cores from each site. The x-radiograph is used to interpret the fine-scale sedimentary fabric of the sediment cores (Fig. 4.9a). In this x-ray negative image, high density objects such as carbonate shells (density *c.* 2.5 g cm^{-3}) appear white whereas low-density and fine-grained mud appear as various shades of grey. Low-density organic material such as wood or peat (density *c.* $<0.5 \text{ g cm}^{-3}$) can appear almost black.

The particle size distribution (PSD) of the sediments is described by the mean, median and standard deviation summary statistics (Fig. 4.9b). Sediments with symmetrical PSD will have similar median and mean particle sizes whereas PSD with fine or coarse tails will not.

Figure 4.9c shows the dry-bulk sediment density (DBD, g cm^{-3}). Sediments composed of quartz or feldspar sand will have DBD values of *c.* $\geq 2 \text{ g cm}^{-3}$. By comparison, estuarine muds composed of clay and silt (i.e., $\leq 63 \mu\text{m}$) have wet-bulk sediment densities of $1\text{--}1.2 \text{ g cm}^{-3}$ and DBD values of $\leq 1 \text{ g cm}^{-3}$. In the present study, DBD profiles are relatively uniform at *c.* 0.5 g cm^{-3} , with porosities of *c.* 80% assuming a particle density of 2.6 g cm^{-3} . This means that 80% of the wet-sediment volume is composed of water. Bulk density increases with depth in the sediment column as sediments are gradually buried, compacted and de-watered by the weight of overlying sediments. DBD profiles can be uniform when sedimentation is rapid (i.e., 10s mm yr^{-1}) and/or insufficient time has elapsed for sediment compaction and dewatering. This is the case in the present study.

$^{210}\text{Pb}_{\text{us}}$ and ^{137}Cs profiles provide information on time-averaged SAR (Figs. 4.9d & e) and are used to interpret how the mud flat has developed over the last 100 years

before, during and after mangrove colonisation in the mid-1950s. The age of the sediments at inflection points in the $^{210}\text{Pb}_{\text{us}}$ profile are also shown. These inflection points indicate changes in the sediment accumulation rate.

4.3.3 Site LC-3 (old-growth forest)

Site LC-3 is located 305 metres seaward of the stopbank in the old-growth forest and close to site of initial mangrove colonisation at Transect B (Fig. 4.8). Replicate core LC-3B was driven to 192 cm, with 183 cm retained. Results for core LC-3B are presented here.



Figure 4.8: Location of core LC-3 in old growth mangrove. View looking north (22 February 2005).

Figure 4.9a shows the x-radiograph for core LC-3B. An enlarged view of the upper 40-cm of core LC-3B shows this structure in more detail (Fig. 4.10). The sediment contains cm-scale horizontal roots and more numerous mm-scale fine roots that show as black threads. In *Avicennia* mangrove species, horizontal roots are known as cable roots (Fig. 4.10, 9-cm depth) and the more numerous smaller-diameter offshoot roots are known as laterals or anchor roots. A feature of the x-radiograph image is the white-coloured band between 20–80cm depth, which is indicative of relatively high density and/or coarse materials such as sand and shell. Weakly laminated sediments occur at 95–140-cm depth composed of discontinuous mm-thick sand layers inter-layered between cm-thick layers silt (Fig. 4.9a). Below 150-cm depth, layers of sand and shell hash occur at 150–155 and 160–183-cm depth. These layers also contain whole valves of the estuarine trough shell (*Macra ovata*), which is a suspension-feeding bivalve characteristic of estuarine intertidal flats.

LC-3B sediments are composed of homogeneous silts, with negligible down-core variation in particle-size statistics. Median (D_{50}) particle diameter varies between 8 μm and 14 μm (Fig. 4.9b). DBD is also uniform down core and varies about an average value of 0.47 g cm^{-3} (Fig. 4.9c) and indicates that there has been negligible compaction of these sediments after deposition. Peaks in DBD below 130-cm depth of 0.6–0.7 g cm^{-3} coincide with shell-hash layers.

The particle-size and DBD data for LC-3B indicate that the sediment is composed of low-density silt. These results are inconsistent with the apparent high density layer at 20–80-cm depth indicated by the x-radiograph. Mangrove roots release oxygen into the anaerobic substrate precipitating iron and manganese oxides on the root surfaces (Dr Brian Sorrell, NIWA, pers. comm.). These precipitates can persist in the sediment after roots have decayed. This biogeochemical process is commonly observed in wetland plants, including mangroves (Kristensen and Alongi, 2006).

Core LC-3B displays a prominent $^{210}\text{Pb}_{\text{us}}$ stair-step profile that indicate changes in time-averaged SAR over time (Fig. 4.9d). The changes in SAR indicated by the $^{210}\text{Pb}_{\text{us}}$ profile are consistent with the aerial-photographic record, which shows that the site was colonised by mangroves during the period 1952 to 1963.

In the lowermost section of the core, below 120-cm depth, SAR average 21 mm yr^{-1} . This section of the core coincides with the time period before the mid-1950s, as indicated by the maximum depth of ^{137}Cs penetration at 129 cm. ^{137}Cs deposition from the atmosphere first occurred in New Zealand in 1953. ^{137}Cs deposition in estuaries from the atmosphere would have been immediate whereas there is likely to have been a small delay in ^{137}Cs delivery associated with eroded top-soil (Appendix One). The aerial photographs show that this lower section of the core coincides with a 30-year period before initial mangrove colonisation of the mud flats. The basal sediments were deposited in the mid-1920s.

The onset of mangrove colonisation of the mudflat near site LC-3 in the mid-1950s is clearly shown by the abrupt increase in SAR indicated by the $^{210}\text{Pb}_{\text{us}}$ profile at 120-cm depth (Fig. 4.9d). SAR increased to 57 mm yr^{-1} and deposited *c.* one metre of sediment over the next *c.* 15 years. This period of elevated SAR coincides with the location of the seaward edge or fringe of the mangrove forest near site LC-3.

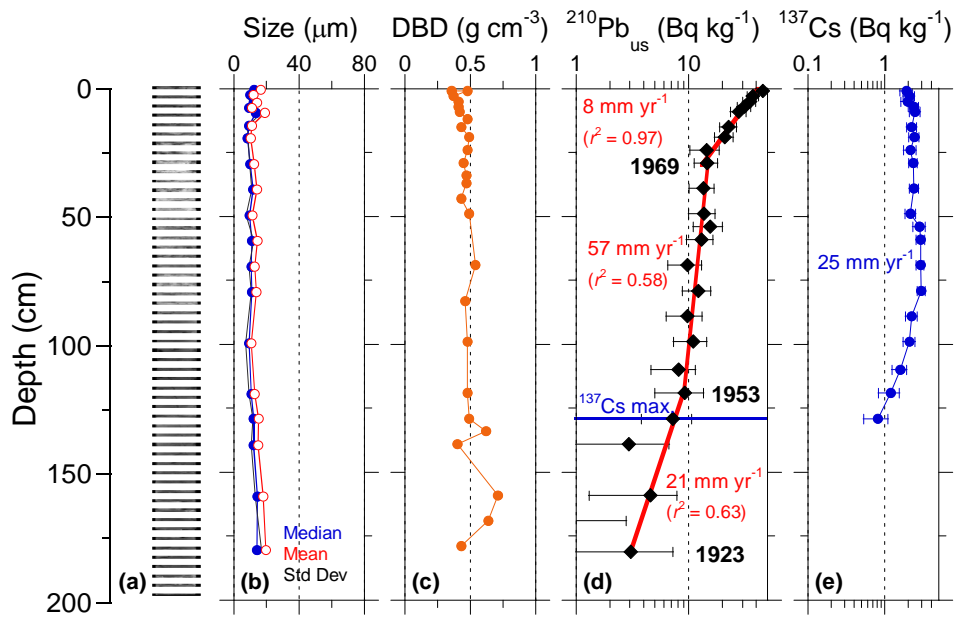


Figure 4.9: Core LC-3 (old-growth forest) sediment profiles: (a) x-radiograph; (b) particle diameter statistics; (c) dry-bulk sediment density; (d) unsupported ^{210}Pb concentrations with 95% confidence intervals shown. Time-averaged sediment accumulation rate (SAR) and co-efficient of determination (r^2) derived from fit to data (red line) and maximum ^{137}Cs depth. Also shown are the ages of the sediment deposit at inflection points in the ^{210}Pb profile; (e) ^{137}Cs concentration profile with 95% confidence intervals shown and time averaged SAR. Note: Fig. (a) x-axis is twice normal scale.

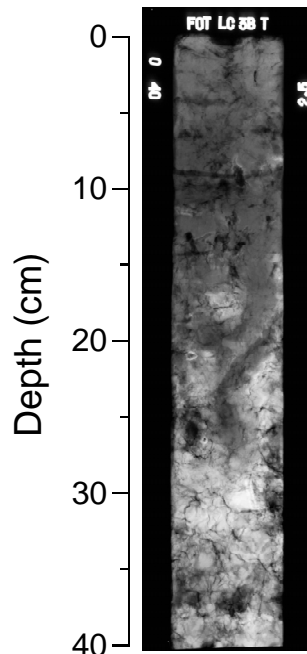


Figure 4.10: X-radiograph Core LC-3B, 0 to 40-cm depth.

Further seaward expansion of the mangrove forest between 1963 and 1977 (Fig. 4.3a) is indicated by the abrupt decrease in the $^{210}\text{Pb}_{\text{us}}$ SAR to 8 mm yr^{-1} at 30-cm depth. After event two the old-growth mangrove forest at LC-3 was progressively isolated from the sea and the supply of sediment provided by the mud flat. The $^{210}\text{Pb}_{\text{us}}$ data indicate that event two began in the mid-1960's.

Figure 4.9e shows the ^{137}Cs profile for core LC-3B. The ^{137}Cs SAR of 25 mm yr^{-1} represents an average rate of sedimentation over the last *c.* 50 years. The $^{210}\text{Pb}_{\text{us}}$ profile shows that SAR have varied considerably during this time period due to mangrove colonisation and forest expansion.

4.3.4 Site LC-4 (old-growth forest)

Site LC-4 is collected 400 metres seaward of the stopbank on former mudflat that was colonised by mangroves from the early 1950's (event one). Replicate core LC-4A was driven to 191 cm, with 178-cm retained. Results for core LC-4A are presented here.

The x-radiograph for core LC-4A shows cable roots and numerous fine lateral roots in a matrix of apparent high-density sediment in the top 50-cm of the sediment column (Fig. 4.11a). This sediment fabric is similar to site LC-3. Weakly laminated sediments occur below 100-cm at 100–120 and 140–180-cm depth (Fig. 4.11a). These sediments are composed of discontinuous mm-thick sand units inter-layered between the homogeneous silt. The core also contains several shells of the mudflat whelk (*Cominella glandiformis*). Like LC-3, site LC-4 shows negligible down-core variation in particle size. Median (D_{50}) particle diameter varies between 7 and $16 \mu\text{m}$ (Fig. 4.11b). The DBD profile shows no clear trend down core and varies about an average value of 0.54 g cm^{-3} (Fig. 4.11c). The uniform DBD profile indicates that there has been negligible compaction of these sediments.

The $^{210}\text{Pb}_{\text{us}}$ profile for site LC-4 is similar to LC-3B and displays a characteristic stair-step profile which indicate abrupt changes in sedimentation rates (Fig. 4.11d). The changes in SAR indicated by the $^{210}\text{Pb}_{\text{us}}$ profile are consistent with the aerial-photographic record, which shows that the site was colonised by mangroves during the period 1963 to 1977. The oldest sediments, below 120-cm depth, were deposited during the late 1930s to mid-1960s. These dates are consistent with the presence of ^{137}Cs to 149 cm depth. During this period SAR averaged 22 mm yr^{-1} .

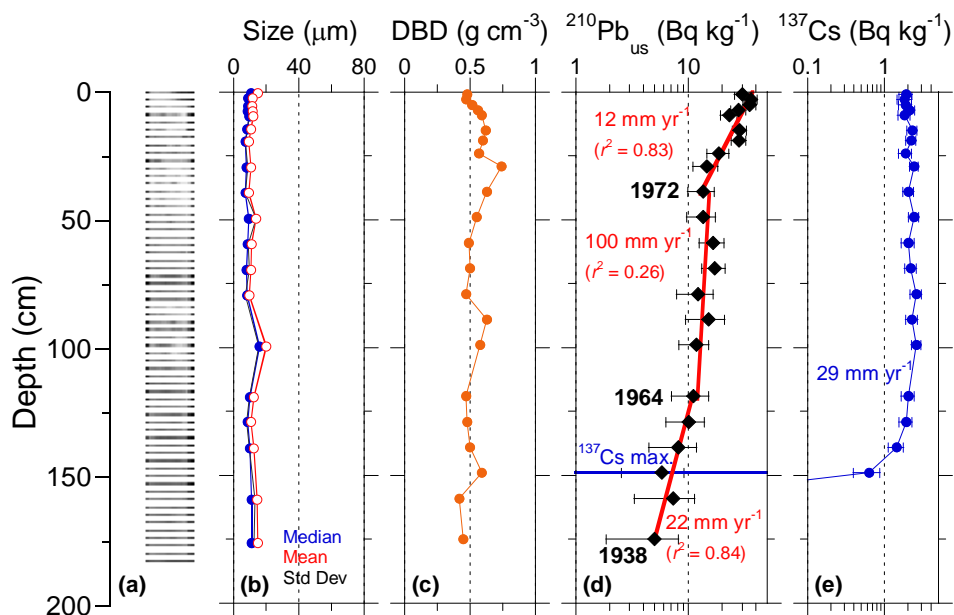


Figure 4.11: Core LC-4A sediment profiles: (a) x-radiograph; (b) particle diameter statistics; (c) dry-bulk sediment density; (d) unsupported ^{210}Pb concentrations with 95% confidence intervals shown. Time-averaged sediment accumulation rate (SAR) and co-efficient of determination (r^2) derived from fit to data (red line) and maximum ^{137}Cs depth. Also shown are the ages of the sediment deposit at inflection points in the ^{210}Pb profile; (e) ^{137}Cs concentration profile with 95% confidence intervals shown and time averaged SAR. Note: Fig. (a) x-axis is twice normal scale.

The onset of mangrove colonisation at LC-4 from the mid-1960s onwards is indicated by the abrupt increase in SAR to 100 mm yr^{-1} at 120-cm depth (Fig. 4.11d). Some 0.8 m of mud was deposited at LC-4 over an eight year period, while the mangrove-forest fringe occupied this site. Further seaward expansion of the mangrove forest after *c.* 1972 is indicated by the abrupt decrease in the $^{210}\text{Pb}_{\text{us}}$ SAR to 12 mm yr^{-1} at 30-cm depth. The old-growth mangrove forest in the vicinity of site LC-4 was progressively isolated from the sea and the supply of sediment provided by the mud flat. Figure 4.8e shows the ^{137}Cs profile for core LC-4A. The ^{137}Cs SAR of 29 mm yr^{-1} represents an average rate of sedimentation over the last *c.* 50 years.

4.3.5 Site LC-5 (old-growth forest)

Site LC-5 is located 501 metres seaward of the stopbank on former mudflat that was colonised by mangroves during the period 1963–1977 (Fig. 4.3a). The tallest mangrove trees occur here between 450–550 m seaward of the stopbank, with an average canopy height of *c.* 3 m (Fig. 4.12). The substrate surface is covered by

decomposing mangrove leaves and branches. Replicate core LC-5A was driven to 189 cm, with 183-cm retained. Results for core LC-5A are presented here.



Figure 4.12: Site LC-5. The tallest mangrove trees occur between 450 and 550 m from the stopbank (photos: January 2006).

The x-radiograph for core LC-5A is similar to the previous cores, with numerous fine lateral roots with high-density precipitates that form halos. A gradual down-core increase in sediment density is inferred from the progressively lighter-hue of the x-ray image with depth (Fig. 4.13a). Laminated beds composed of discontinuous mm-thick sand units inter-layered with silt occur below 150-cm depth. Figure 4.14 shows the x-radiograph for the bottom 24-cm of core LC-5A. These laminated sand and silts are characteristic of energetic mixed-sediment intertidal environments in estuaries and bays (Rhineck and Singh, 1980).

The gradual down-core increase in sediment density indicated by the x-radiographs, is supported by the particle-size profiles. Median particle diameter increases from 9 μm at the surface to 15 μm in the basal sediments (Fig. 4.13b). The apparent increase in sediment density indicated by the x-radiograph is not supported by the DBD profile, which shows no clear trend with depth. The average DBD value is 0.48 g cm^{-3} (Fig. 4.13c). The uniform DBD profile indicates that there has been negligible compaction of these sediments.

The $^{210}\text{Pb}_{\text{us}}$ profile for site LC-5 is again similar to LC-3 and LC-4, with the characteristic stair-step profile indicating abrupt changes in sedimentation rates (Fig. 4.13d). The aerial-photographs show that site LC-5 was colonised by mangroves

during the period 1963 to 1977. In the oldest sediments below 120-cm depth, SAR average 10 mm yr⁻¹ between the late-1920s to late-1950s. These dates are consistent with the presence of ¹³⁷Cs to 149 cm depth, which is during the deposition period estimated from the ²¹⁰Pb_{us} SAR.

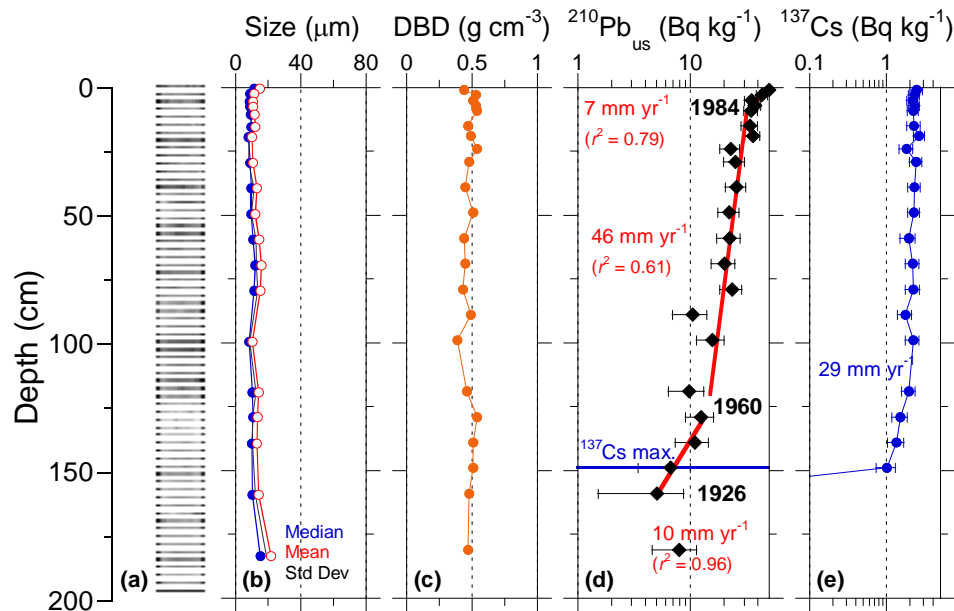


Figure 4.13: Core LC-5A sediment profiles: (a) x-radiograph; (b) particle diameter statistics; (c) dry-bulk sediment density; (d) unsupported ²¹⁰Pb concentrations with 95% confidence intervals shown. Time-averaged sediment accumulation rate (SAR) and co-efficient of determination (r^2) derived from fit to data (red line) and maximum ¹³⁷Cs depth. Also shown are the ages of the sediment deposit at inflection points in the ²¹⁰Pb profile; (e) ¹³⁷Cs concentration profile with 95% confidence intervals shown and time averaged SAR. Note: Fig. (a) x-axis is twice normal scale.

The onset of mangrove colonisation at LC-5 from *c.* 1960 onwards is shown by the increase in SAR to 46 mm yr⁻¹ at 120-cm depth (Fig. 4.13d), with *c.* 1.1 metres of sediment was deposited over the next 25 years. This date for initial colonisation is earlier than indicated by the 1963 aerial photograph. The period of rapid sedimentation coincides with mangrove colonisation and forest development. The abrupt decline in SAR to 7 mm yr⁻¹ after *c.* 1984 (30-cm depth) followed major forest expansion seaward of site LC-6 that is captured by the 1987 aerial photograph. Following this event, LC-5 was progressively isolated by elevation and distance from the supply of sediment provided by the mud flat. Figure 4.13e shows the ¹³⁷Cs profile for core LC-5A. The ¹³⁷Cs SAR of 29 mm yr⁻¹ represents an average rate of sedimentation over the last *c.* 50 years.

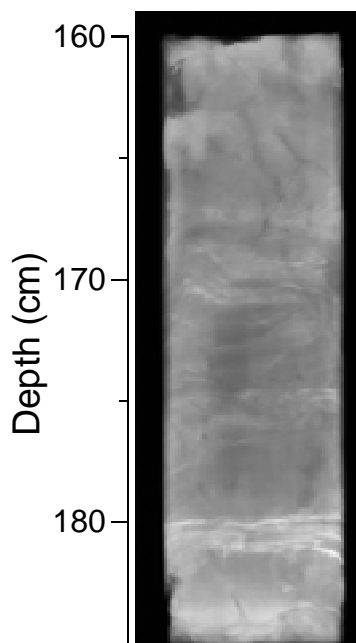


Figure 4.14: X-radiograph of Core LC-5A (depth: 160–184 cm). Sediments near the base of the core are composed of discontinuous mm-thick sand layers inter-bedded with cm-thick silt deposits.

4.3.6 Site LC-6 (old-growth forest)

Site LC-6 is located 565 metres seaward of the stopbank. Forest structure here is distinct from the tall mangrove trees (450–550 m) immediately landwards. The mangrove trees are densely spaced and have single straight trunks to about 2 m height, with steep branches arising from the single straight stem, as opposed to the open growth form of the tall mangroves at LC-5 (Fig. 4.12). This morphology is indicative of trees growing under conditions when light is limiting, as can occur when seedlings are growing under larger trees. The aerial photographs show that site LC-6 occupied the seaward fringe of the mangrove forest in 1977 (Fig. 4.3a). Replicate core LC-6A was driven to 188 cm, with 180-cm retained. Results for core LC-5A are presented here.

The x-radiograph for core LC-6A is similar to the previous cores, with numerous fine lateral roots surrounded by high density precipitates forming halos. A gradual down-core increase in sediment density is inferred from the progressively lighter-hue of the x-ray image with depth (Fig. 4.15a). Laminated beds composed of discontinuous mm-thick sand units inter-layered with silt occasionally occur below 75-cm depth. Shell

valves of *M. ovata* occur at 145 and 160-cm depth. Sediments are composed of homogenous low-density fine silts, with median particle diameters of 8–16 μm (Fig. 4.15b–c). The sediment DBD averages 0.50 g cm^{-3} .

The $^{210}\text{Pb}_{\text{us}}$ profile for site LC-6 differs markedly from the cores previously described. A notable feature of the $^{210}\text{Pb}_{\text{us}}$ profile is the presence of an unconformity at 79–89-cm depth. The difference in $^{210}\text{Pb}_{\text{us}}$ concentration between the top and bottom of the unconformity is 10.9 Bq kg^{-1} . An age difference of *c.* 25 years between these two layers is calculated from the ^{210}Pb decay constant (k , 0.03114 yr^{-1}). The time-averaged SAR of 4 mm yr^{-1} is an order of magnitude lower than for sediments deposited above or below this layer. The origin of this unconformity in LC-6 is discussed in section five.

Core LC-6 also records the transition from a bare mudflat to a mangrove forest. It is difficult to date the onset of mangrove colonisation based on the $^{210}\text{Pb}_{\text{us}}$ data alone because of the unconformity. In the lowermost section of the core, below 159-cm depth, SAR averaged 12 mm yr^{-1} . Sediments in this lower section of the core were deposited on a mudflat during the 1940s–1950s. This is indicated by the presence of ^{137}Cs , to 169 cm depth, in this lower section of the core.

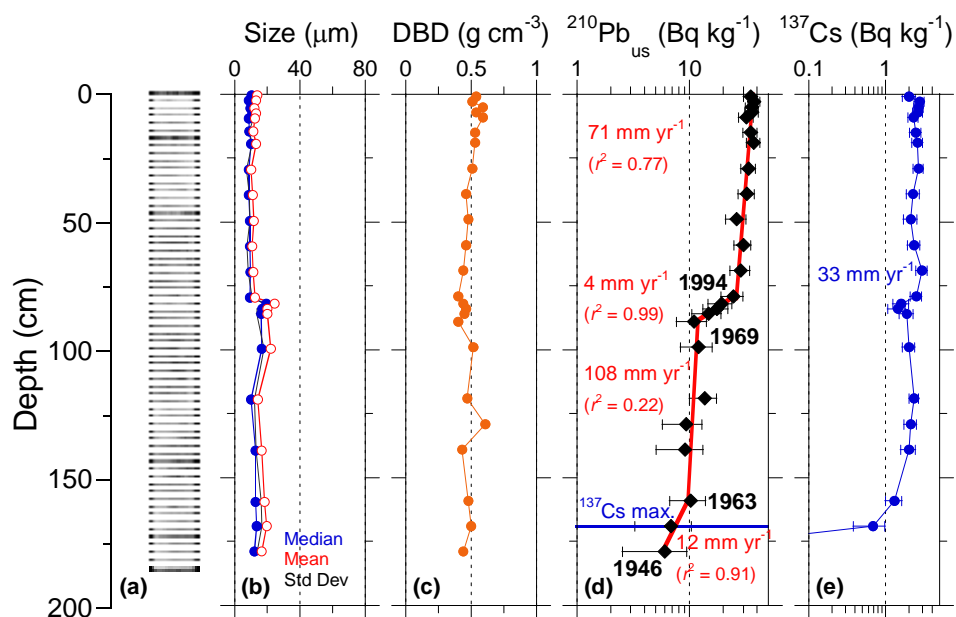


Figure 4.15: Core LC-6A sediment profiles: (a) x-radiograph; (b) particle diameter statistics; (c) dry-bulk sediment density; (d) unsupported ^{210}Pb concentrations with 95% confidence intervals shown. Time-averaged sediment accumulation rate (SAR) and co-efficient of determination (r^2) derived from fit to data (red line) and maximum ^{137}Cs depth; (e)

^{137}Cs concentration profile with 95% confidence intervals shown and time averaged SAR. Note: Fig. (a) x-axis is twice normal scale.

The onset of mangrove colonisation at site LC-6 occurs below the unconformity and is indicated by the abrupt increase in SAR from 12 mm yr^{-1} to 108 mm yr^{-1} at 160-cm depth (Fig. 4.15d). SAR reduces to 71 mm yr^{-1} above the unconformity. Unlike the previous cores there is no evidence of a reduction in SAR as site LC-6 was progressively isolated from the mudflat. The ^{137}Cs SAR of 33 mm yr^{-1} represents an average rate of sedimentation over the last *c.* 50 years (Fig. 4.15e).

4.3.7 Site LC-7 (recent mangrove forest)

Site LC-7 is located 634 metres seaward of the stopbank. The present-day mangrove forest at LC-7 is composed of densely-spaced trees up to 1.5 m in height (Fig. 4.16). Aerial photographs show that site LC-7 was colonised by mangroves in the mid-1980s (Fig. 4.3b). Replicate core LC-7A was driven to 191 cm, with 182-cm retained. Results for core LC-7A are presented here.

The x-radiograph for core LC-7A is similar to previous cores. Numerous fine lateral roots occur in the top 50-cm of the core. Precipitates form halos around these roots in the silt substrate. A gradual down-core increase in sediment density is inferred from the progressively lighter-hue of the x-ray image with depth (Fig. 4.17a). Occasional mm-scale fine-sand layers occur below 80-cm. A shell hash layer occurs at 150–155-cm depth. Below 175-cm depth the homogenous silt is replaced by finely-laminated beds composed of mm-thick fine-sand and silt layers that is characteristic of energetic mixed-sediment intertidal flats. Figures 4.17b–c show that sediments at LC-7 are similar to the homogenous low-density fine silts that characterise cores collected elsewhere in the mangrove forest. Sediment DBD averages 0.49 g cm^{-3} .

The $^{210}\text{Pb}_{\text{us}}$ profile for site LC-7 also records the changes in sedimentation rates that have occurred as the mangrove forest has spread seawards across the mud flats (Fig. 4.17d). The $^{210}\text{Pb}_{\text{us}}$ profile differs from cores LC-3 – LC-5 in that there is a progressive increase in SAR over time, in contrast to the reduction in sediment supply in near-surface sediments. The former mudflat accreted at 8 mm yr^{-1} until *c.* 1964, when SAR increased to 33 mm yr^{-1} . SAR further increased in *c.* 1992 to 56 mm yr^{-1} , which coincides with mangrove colonisation. The aerial photographs show that the initial increase in SAR occurred decades before mangroves colonised site LC-7 (Fig. 4.3). Thus, from the mid-1960s onwards the mudflat began to accrete sediment more rapidly than had previously occurred. By 2006, LC-7 was 300 metres landward of the

seaward edge of the mangrove forest. The ^{137}Cs SAR of 33 mm yr^{-1} represents an average rate of sedimentation over the last *c.* 50 years (Fig. 4.17e).



Figure 4.16: Mangrove forest at site LC-7. View looking north east (23 February 2005).

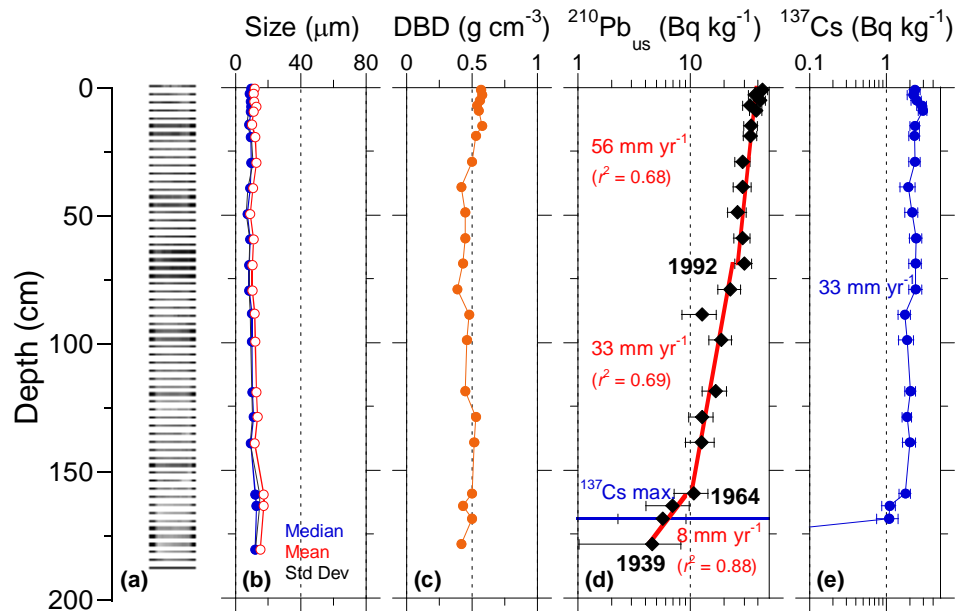


Figure 4.17: Core LC-7A sediment profiles: (a) x-radiograph; (b) particle diameter statistics; (c) dry-bulk sediment density; (d) unsupported ^{210}Pb concentrations with 95% confidence intervals shown. Time-averaged sediment accumulation rate (SAR) and co-efficient of determination (r^2) derived from fit to data (red line) and maximum ^{137}Cs depth. Also shown are the ages of the sediment deposit at inflection points in the ^{210}Pb profile; (e) ^{137}Cs concentration profile with 95% confidence intervals shown and time averaged SAR. Note: Fig. (a) x-axis is twice normal scale.

4.3.8 Site LC-8 (recent mangrove forest)

Site LC-8 is located 726 metres seaward of the stopbank. The mangrove forest here is composed of densely spaced dwarf trees typically < 1 m high (Fig. 4.18). Aerial photographs show that site LC-8 was colonised by mangroves sometime after the mid-1980s (Fig. 4.3b). Replicate core LC-8B was driven to 193 cm depth, with 186-cm retained. Results for core LC-8B are presented here.

Core LC-8B is composed of homogenous fine silt. Numerous fine lateral roots occur in the top 65-cm of the core. (Fig. 4.19) Downward growing primary lateral roots < 1-cm diameter are also observed. Precipitates form halos around these roots in the less-dense silt substrate. Discontinuous mm-scale fine-sand layers occur below 85-cm to the base of the core. Whole and partial shell valves of *M. ovata* occur at 125-cm and 140-cm. The sand content of the sediment increases at the bottom of the core. The profiles show that most of core LC-8B is composed of low-density silt, with basal sediments containing coarse silt and fine sand (Figs. 4.19a–c). Sediment DBD averages 0.50 g cm^{-3} .



Figure 4.18: Dwarf mangroves near site LC-8. View looking south-west (27 January 2006).

The presence of ^{137}Cs at the base of core LC-8B and $^{210}\text{Pb}_{\text{us}}$ ages show that the top 1.9 m of the sediment column has been deposited since the mid-1950s. The former mudflat accreted at 25 mm yr^{-1} until *c.* 1983, when SAR increased to 53 mm yr^{-1} as mangrove colonised the site. Like LC-7, the $^{210}\text{Pb}_{\text{us}}$ profiles shows no evidence that sedimentation rates have reduced as the site has become progressively isolated from the mudflat by distance and elevation. By 2006, LC-8 was 200 metres landward of the seaward edge of the mangrove forest. ^{137}Cs is present to the base of core LC-8 so that the ^{137}Cs -derived SAR of 36 mm yr^{-1} represents a minimum rate over the last 50 years (Fig. 4.19e).

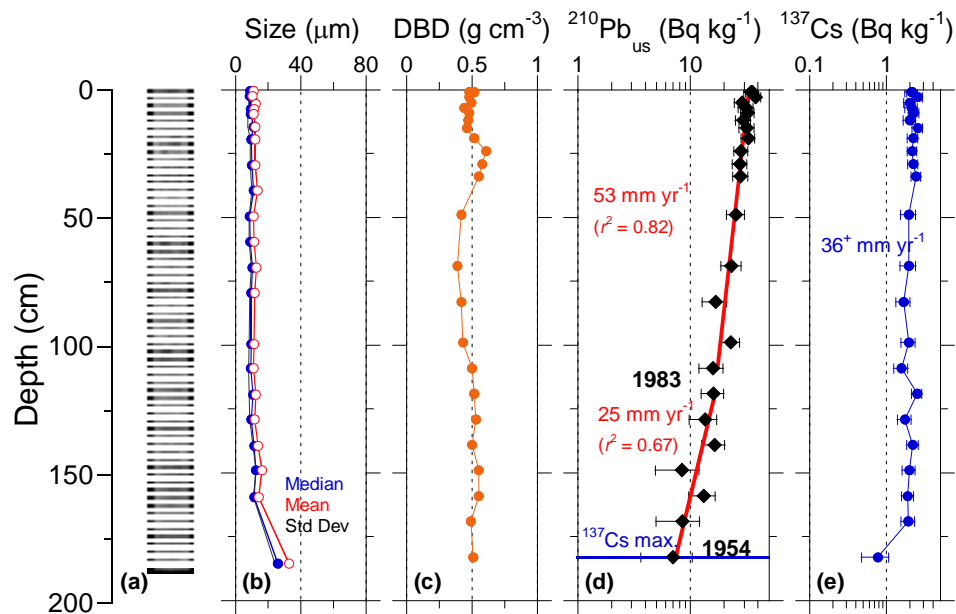


Figure 4.19: Core LC-8B sediment profiles: (a) x-radiograph; (b) particle diameter statistics; (c) dry-bulk sediment density; (d) unsupported ^{210}Pb concentrations with 95% confidence intervals shown. Time-averaged sediment accumulation rate (SAR) and co-efficient of determination (r^2) derived from fit to data (red line) and maximum ^{137}Cs depth. Also shown are the ages of the sediment deposit at inflection points in the ^{210}Pb profile; (e) ^{137}Cs concentration profile with 95% confidence intervals shown and time averaged SAR. Note: Fig. (a) x-axis is twice normal scale.

4.3.9 Site LC-9 (recent mangrove forest)

Site LC-9 is located 814 metres seaward of the stopbank and on the landward side of the present-day mangrove seaward edge. Site LC-9 was colonised by mangroves sometime during the 1987 – 1996 period (Fig. 4.3b). Replicate core LC-9B was driven to 193 cm, with 189-cm retained. Results for core LC-9B are presented here.

The x-radiograph for core LC-9B indicates that sediments are composed of the ubiquitous fine silt as described previously. Numerous fine lateral roots occur in the top 100-cm of the core. (Fig. 4.20). Precipitates form halos around these roots in the less-dense silt substrate. Whole and partial shell valves of *M. ovata* occur at 160–165 and 170–175-cm depth. Discontinuous mm-scale fine-sand layers occur below 160-cm to the base of the core. Particle size increases markedly below 150-cm, with the median size increasing from 10 μm to 50 μm maximum (Fig. 4.17b). The average DBD value of sediments at site LC-9 is 0.49 g cm^{-3} .

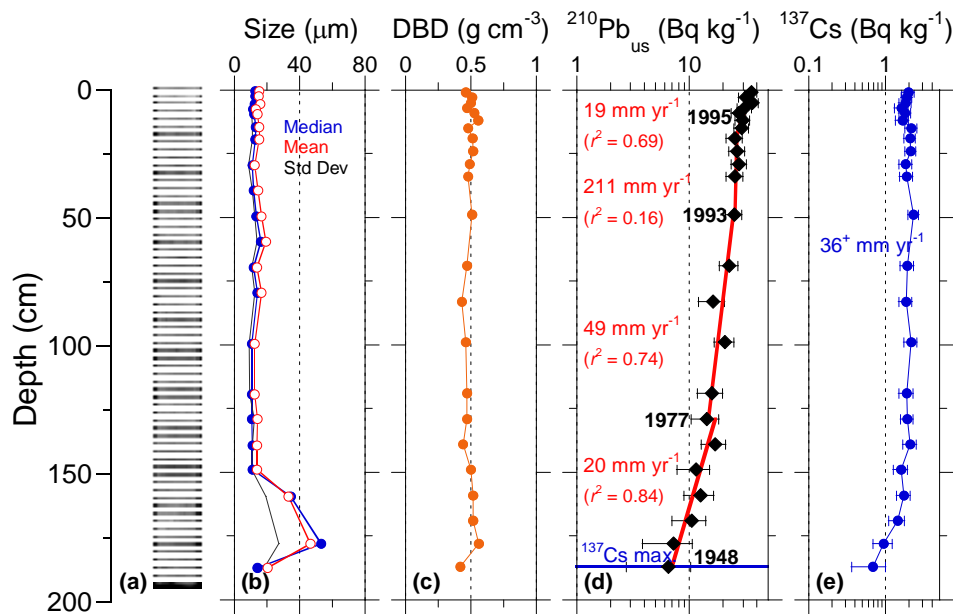


Figure 4.20: Core LC-9B sediment profiles: (a) x-radiograph; (b) particle diameter statistics; (c) dry-bulk sediment density; (d) unsupported $^{210}\text{Pb}_{\text{us}}$ concentrations with 95% confidence intervals shown. Time-averaged sediment accumulation rate (SAR) and co-efficient of determination (r^2) derived from fit to data (red line) and maximum ^{137}Cs depth. Also shown are the ages of the sediment deposit at inflection points in the ^{210}Pb profile; (e) ^{137}Cs concentration profile with 95% confidence intervals shown and time averaged SAR. Note: Fig. (a) x-axis is twice normal scale.

Like LC-8, the presence of ^{137}Cs at the base of core LC-9B and $^{210}\text{Pb}_{\text{us}}$ SAR indicate that these sediments have been deposited since the mid-1950s (Fig. 4.20). The $^{210}\text{Pb}_{\text{us}}$ profile is more complex than the simple stair-step form previously described. Sedimentation rates on the former mudflat increased from 20 mm yr^{-1} to 49 mm yr^{-1} in *c.* 1977. Thus, the mudflat began to accrete sediment more rapidly in the mid-1970s and at least 10 years before mangroves colonised the site.

The onset of mangrove colonisation at site LC-9 is indicated by the abrupt increase in SAR to 211 mm yr^{-1} at 50-cm depth and *c.* 1993. An apparent ten-fold decline in SAR to 19 mm yr^{-1} occurred after 1995. LC-9 is now *c.* 90 m from the seaward edge of the forest fringe (Fig. 4.3b). ^{137}Cs is present to the base of core LC-9B so that the average ^{137}Cs -derived SAR of 36 mm yr^{-1} represents a minimum value over the last *c.* 50 years (Fig. 4.20e).

4.3.10 Site LC-10 (recent mangrove forest)

Site LC-10 is located 902 metres seaward of the stopbank in the tall mangrove near the present seaward edge of the mangrove forest (Fig. 4.21). Site LC-10 was located on the seaward edge of the mangrove forest in 1996 (Fig. 4.3b). Replicate core LC-10B was driven to 190 cm, with 183-cm retained. Results for core LC-10B are presented here.



Figure 4.21: Tall mangroves near the present-day seaward edge of the mangrove forest at site LC-10. View looking north to the Firth of Thames (22 February 2005).

Unlike cores collected from the older mangrove forest, the x-radiograph for LC-10 shows that mangrove lateral roots and associated oxide precipitates are largely absent (Fig. 4.22a). The top 130-cm of the sediment column is composed of homogenous fine silt. Below this depth there is an abrupt transition to a sequence of laminated fine-sands and silts. These beds progressively increase in scale from mm to cm-thick layers with depth (Fig. 4.23). Whole and partial shell valves of *M. ovata* are abundant in the bottom-most sediments at 160–183-cm depth. These laminated beds, characteristic of energetic mixed-sediment intertidal environments, have been previously noted in the LC cores but are much more distinct at site LC-10. This transition to coarser-laminated sediments is also shown by the marked increase in

particle size below 75- μm . Median-particle size increases from 12 μm to 68 μm maximum (Fig. 4.22b). Peaks in the DBD profile mirror the down-core particle-size variations (Fig. 4.22c).

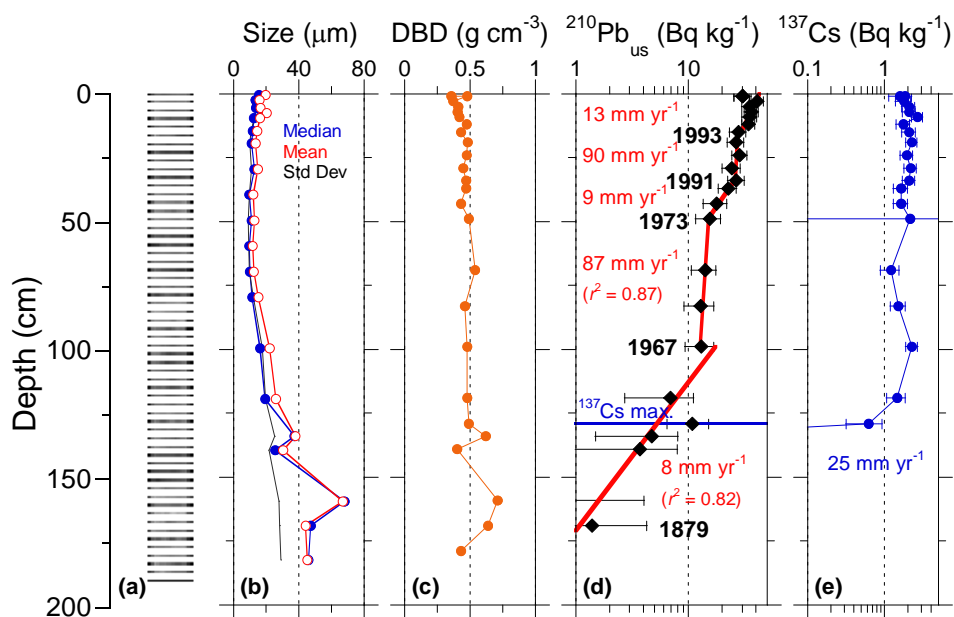


Figure 4.22: Core LC-10B sediment profiles: (a) x-radiograph; (b) particle diameter statistics; (c) dry-bulk sediment density; (d) unsupported ^{210}Pb concentrations with 95% confidence intervals shown. Time-averaged sediment accumulation rate (SAR) and co-efficient of determination (r^2) derived from fit to data (red line) and maximum ^{137}Cs depth. Also shown are the ages of the sediment deposit at inflection points in the ^{210}Pb profile; (e) ^{137}Cs concentration profile with 95% confidence intervals shown and time averaged SAR. Note: Fig. (a) x-axis is twice normal scale.

Because LC-10 is located on the seaward-sloping mud beach at a lower surface elevation so that core LC-10 samples older sediments down to -0.65 m MSL. ^{210}Pb dating indicates that these basal sediments were deposited in the 1880s. The $^{210}\text{Pb}_{\text{us}}$ profile is of a complex stair-step form (Fig. 4.22d). Sedimentation rates on the former mudflat increased tenfold from 8 to 87 mm yr^{-1} after *c.* 1967 and occurred 30 years before mangroves colonised the site. This period of rapid mudflat accretion continues until *c.* 1973 when SAR decline to 9 mm yr^{-1} . The onset of mangrove colonisation at site LC-10 is indicated by an increase in SAR to 90 mm yr^{-1} between 1991 and 1993. Since that time SAR have averaged 13 mm yr^{-1} . By 2006, site LC-10 was *c.* 50 m from the seaward edge of the forest fringe (Fig. 4.3b). The ^{137}Cs SAR has averaged 25 mm yr^{-1} over the last *c.* 50 years (Fig. 4.22e).

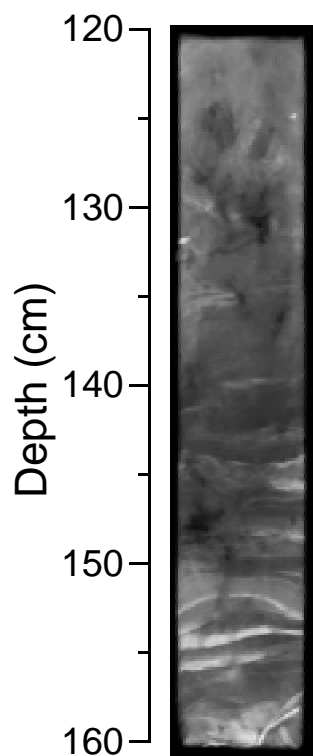


Figure 4.23: X-radiograph of Core LC-10B, 120–160cm depth. The transition from homogenous fine silt to laminated beds of fine sand and silt below 130-cm depth is clearly shown.

4.3.11 Site LC-11 (2005 forest fringe)

Site LC-11 is located 930 metres seaward of the stopbank in the tall mangrove near the present seaward edge of the mangrove forest (Fig. 4.24). In 1996, Site LC-11 was located on the mudflat and *c.* 20 m seaward of the fringe. The 1996 aerial photograph indicates that juvenile mangrove were present on the mudflat around LC-11 (Fig. 4.3b). Replicate core LC-11A was driven to 192 cm, with 181-cm retained. Results for core LC-11A are presented here.

The x-radiograph shows that the top 80-cm of core LC-11 is composed of homogenous fine silt (Fig. 4.25a). Occasional laminated mm-scale sand layers occur below 40-cm depth. These laminated sand and mud layers are abundant below 80-cm depth. Whole and partial shell valves of *M. ovata* occur below 95-cm depth. These laminated beds progressively increase in scale from mm to cm-thick layers with depth.

These units are the same as those described in core LC-10 (Fig. 4.23). This transition to coarser-laminated sediments is also shown by the marked increase in particle size below 75-cm. Median-particle size increases from 12 μm to 68 μm maximum (Fig. 4.25b). The uniform DBD profile indicates that there has been negligible compaction of these sediment deposits (Fig. 4.25c).



Figure 4.24: View of site LC-11 at seaward edge of the mangrove forest (22 February 2005).

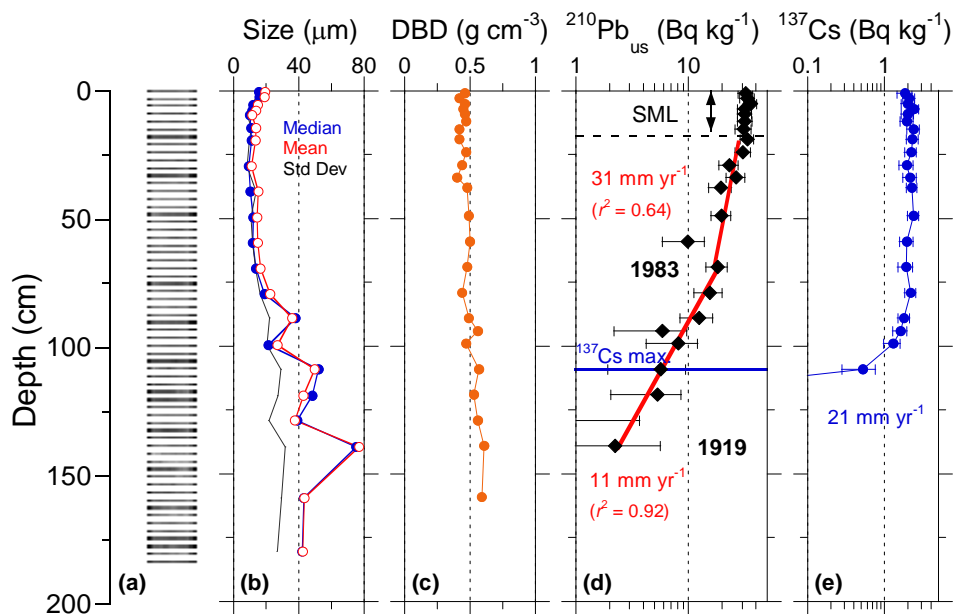


Figure 4.25: Core LC-11A sediment profiles: (a) x-radiograph; (b) particle diameter statistics; (c) dry-bulk sediment density; (d) unsupported ^{210}Pb concentrations with 95% confidence intervals shown. Time-averaged sediment accumulation rate (SAR) and co-efficient of determination (r^2) derived from fit to data (red line) and maximum ^{137}Cs depth.

Also shown are the ages of the sediment deposit at inflection points in the ^{210}Pb profile; (e) ^{137}Cs concentration profile with 95% confidence intervals shown and time averaged SAR. Note: Fig. (a) x-axis is twice normal scale.

LC-11 was sampled from the mudflat several metres seaward of the forest fringe in January 2005. The core samples sediments down to -0.67 m MSL. ^{210}Pb dating indicates that these basal sediments were deposited in *c.* 1919. The $^{210}\text{Pb}_{\text{us}}$ profile indicates a three-fold increase in SAR from 11 mm yr^{-1} to 31 mm yr^{-1} in the early 1980s (Fig. 4.25d). The ^{137}Cs SAR has averaged 21 mm yr^{-1} over the last *c.* 50 years (Fig. 4.25e).

The uniform $^{210}\text{Pb}_{\text{us}}$ concentrations in the top 20-cm of the sediment column indicate a surface-mixed layer (SML). The maximum residence time of sediment particles within the SML is *c.* 7 years (i.e., SML/SAR). Sediments are eventually removed from the SML by burial due to sedimentation. The depth of the SML scales with the height of the large-scale mudforms that mantle the mudflat adjacent to the mangrove-forest.

4.3.12 Site LC-12 (mudflat)

Site LC-12 is located 978 metres seaward of the stopbank on the mudflat 50 m seaward of the mangrove-forest fringe (i.e., January 2005, Fig. 4.26). Replicate core LC-12A was driven to 70 cm, with 70-cm retained. Results for core LC-21A are presented here.



Figure 4.26: View of site LC-12 on the mudflat *c.* 50 m seaward of the mangrove-forest fringe (22 February 2005).

Mudflat sediments to 70-cm depth are composed of homogenous muds. The uniform DBD profile indicates that there has been negligible compaction of these sediment deposits (Fig. 4.27a). Uniform $^{210}\text{Pb}_{\text{us}}$ concentrations in the top 20-cm of the sediment column indicate a SML (Fig. 4.27b). Below the SML, the time-average SAR is 25 mm yr^{-1} , so that basal sediments at 70-cm were deposited in the mid-1970s. The maximum residence time of sediment particles within the SML is 8 years. Sediments are removed from the SML by burial due to sedimentation. The depth of the SML scales with the height of the large-scale mudforms that mantle the mudflat adjacent to the mangrove-forest. Because ^{137}Cs occurs to the base of the core, the ^{137}Cs SAR of 13 mm yr^{-1} is an underestimate (Fig. 4.27c).

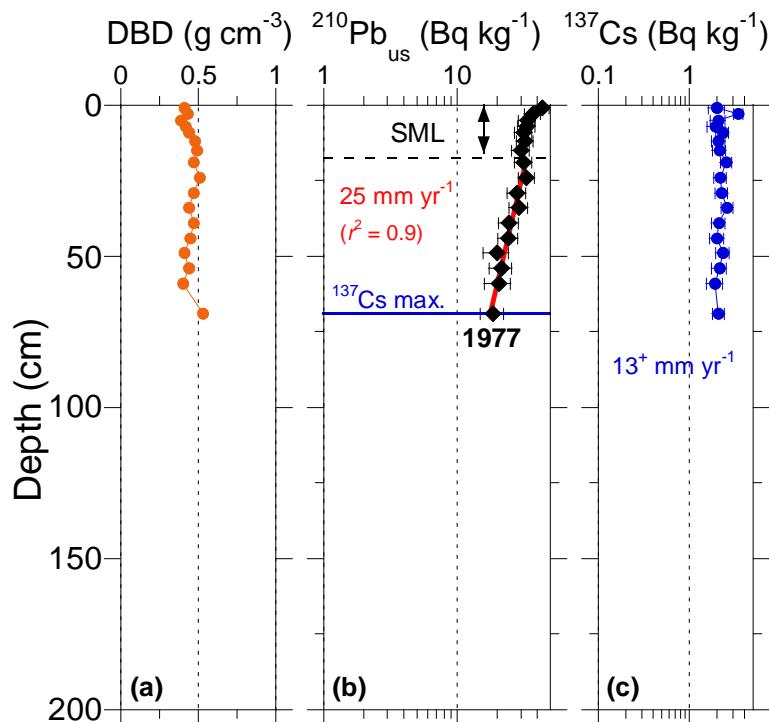


Figure 4.27: Core LC-12A sediment profiles: (a) dry-bulk sediment density; (b) unsupported ^{210}Pb concentrations with 95% confidence intervals shown. Time-averaged sediment accumulation rate (SAR) and co-efficient of determination (r^2) derived from fit to data (red line) and maximum ^{137}Cs depth.; (c) ^{137}Cs concentration profile with 95% confidence intervals shown and time averaged SAR. Note: Fig. (a) x-axis is twice normal scale.

4.3.13 Pollen profiles

The sediment cores were pollen-rich, with generally good pollen preservation (i.e., relatively little biological corrosion). However, many of the pollen grains and spores throughout the cores were abraded and fragmented. Fragmentation was shown mainly by the larger pollen types, namely kauri (*Agathis australis*), pine (*Pinus*), rimu (*Dacrydium*), undifferentiated conifers, Restionaceae, bracken, *Cyathea* and *Dicksonia*. The pollen sum in all cores is dominated by pine, rimu and other native conifers, bracken and *Cyathea* tree ferns (Fig. 4.25 and Appendix Two). Most other pollen types, including mangrove (*Avicennia*) are present in trace quantities and are mainly pollen of native species. Significant exotic pollen types include pine, willow (*Salix*), wattle (*Acacia*), dandelion (*Taraxacum*), docks/sorrel (*Rumex*), grasses (Poaceae) and plantain (*Plantago*).

Several temporal, (i.e., up-core) trends are apparent in the pollen profiles. Mangrove pollen is present in trace quantities in many of the cores above 80-cm depth, although not present in cores LC-7A, LC-10B and LC-11A. Wattle pollen was also found at or above 80-cm depth in cores LC-5A, LC-6A, LC-7A and LC-9B. Pine and grass-pollen content increases up core whereas bracken-spore content generally decreases. Figure 4.25 presents the pollen profiles preserved in core LC-3. Pollen profiles for the remaining cores LC-4 to LC-11 are presented in Appendix Two.

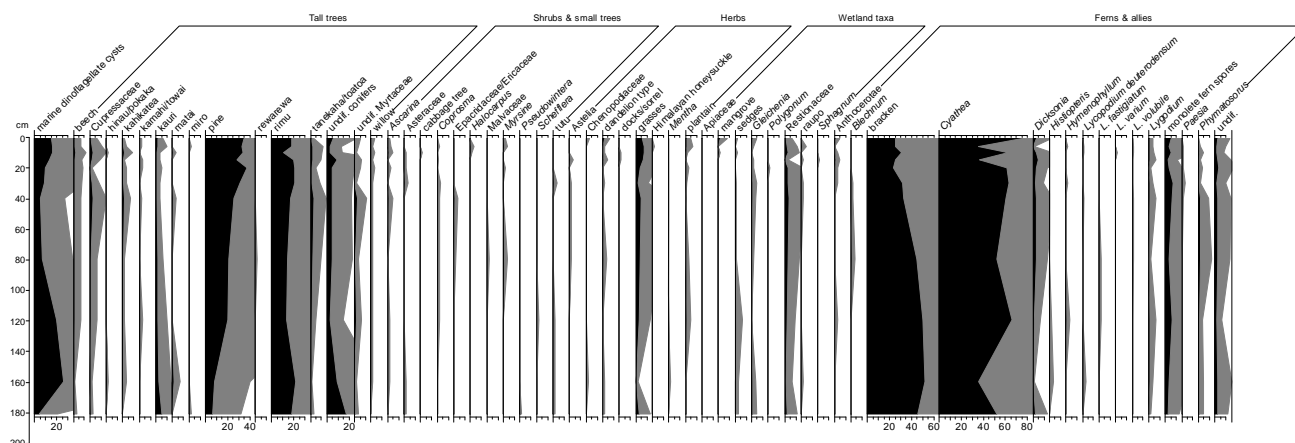


Figure 4.25: Core LC-3 pollen profiles for major plant groups expressed as a percentage of the terrestrial pollen and spore sum.